PISTON SLAP NOISE -- ITS TRANSFER THROUGH AN INTERNAL COMBUSTION ENGINE

Tetsuro Oguchi

B.S. Tokyo University

(1972)

Submitted in Partial Fulfillment

of the Requirements for the Degree of

Master of Science

at the

Massachusetts Institute of Technology

February, 1979

Signature of Author... **Signature redacted**
Department of Mechanical Engineering, Jan. 22, 1979

Certified by.. **Signature redacted**
Thesis Supervisor

Signature redacted

Accepted by..
Chairman, Departmental Committee on Graduate Students

PISTON SLAP NOISE --

ITS TRANSFER THROUGH AN INTERNAL COMBUSTION ENGINE

by

Tetsuro Oguchi

Bs. ME Tokyo Univ. 1972

ABSTRACT

Piston slap noise, which is generated by the sudden impact of the piston on the cylinder wall, is the most predominant mechanical noise emitted from the engine. It is studied here in terms of its transmission paths through the engine elements. Two engines with different cylinder liner types are tested in a non-running condition. The transmission paths are measured and evaluated in terms of the mechanical mobility, the ratio of the velocity response on the cylinder wall to the force applied to the external surface of the engine, which represents, by reciprocity, the ratio of the velocity response on the external surface of the engine to the force applied to the cylinder wall. The work concentrates on the major transmission path of the piston slap noise and the factors which affect that transfer mobility in the frequency range of 1.5 - 4 kHz.

The major transmission path of the piston slap noise is experimentally determined to be the path through the cylinder wall and the upper deck of the cylinder block to the external surface of the cylinder block. The cylinder head and oil pan show less important paths for transmitting piston slap energy. The factors which may affect the transmission path are the various types of damping introduced by assembling the engine parts to the cylinder block as well as the vibrational coupling between various components in the transmission path.

A beam model is introduced to explain the dominant peak of the mobility magnitude and the difference in the corresponding frequency range for each engine. The model studies of the transmission path as well as studies of the effect of damping and coupling should be pursued in order to achieve further reduction of radiated piston slap noise.

Thesis Supervisor: Richard H. Lyon

Title: Professor, Department of Mechanical Engineering

ACKNOWLEDGEMENTS

TABLE OF CONTENTS (CONTINUED)

TABLE OF CONTENTS (CONTINUED)

LIST OF FIGURES

CHAPTER 1

INTRODUCTION

1.1 Noise Problems

Recently the manufacturers who produce moving apparatus of various kinds, most commonly motor vehicles and other transportation devices, have become concerned about the noise produced by their products. This is because of increasing federal and local noise legislation concerned with environmental impact and operator protection. Manufacturers now compete with each other by advertising the quietness of their products.

Since these apparatus are powered by internal combustion engines, this noise legislation affects the design of engine-related components. For example, the noise sources of the highway truck are tires, air intake system, exhaust system, engine cooling system, transmission and chassis. All of these except for tires and transmission are considered to be engine related components. For each of those components, various projects have been carried out and the successful techniques in noise reduction have been reported [1,2,3,4,5]. The component-basis study is rather easier than handling the engine itself because of its simplicity of structure and clearness of noise sources.

```
                                    ┌─ TWO CYCLE
                        ┌─ CYCLE ───┤
                        │           └─ FOUR CYCLE
                        │
                        │                              ┌─ IN-DIRECT INJECTION
                        │               ┌─ DIESEL ─────┤
                        │               │              └─ DIRECT INJECTION
                        │   COMBUSTION  │
COMBUSTION SYSTEM ──────┼─  TYPE ───────┤                  ┌─ CONVENTIONAL
                        │               │                  │   CARBURETION
                        │               └─ SPARK ──────────┤
                        │                  IGNITION        └─ STRATIFIED CHARGE
                        │
                        │                   ┌─ GASOLINE
                        └─ FUEL ────────────┼─ DIESEL
                                            └─ GAS ( PROPANE )


                                            ┌─ RECIPROCATING
POWER TRANSFER MECHANISM ───────────────────┤
                                            └─ ROTARY


                                            ┌─ NATURALLY ASPIRATED
ASPIRATION ─────────────────────────────────┤
                                            └─ TURBOCHARGED


                                            ┌─ HIGH SPEED
                                            │   ( GREATER THAN 3000 rpm )
OPERATING SPEED RANGE ──────────────────────┤
                                            └─ LOW AND MEDIUM SPEED
                                                ( LESS THAN 3000 rpm )
```

FIGURE 1.1 :   INTERNAL COMBUSTION ENGINE CATEGORIZATION

For passenger car engines, the gasoline engine (naturally aspirated) is the most popular, but since the oil crisis, diesel engines are becoming more popular in this market due to their lower fuel consumption. For truck engines, both gasoline and diesel engines are used in North America and mostly diesel engines are used in other countries. For truck diesel engines, turbocharging is widely accepted because of increased specific power [6]. A two cycle engine is thermodynamically superior to a four stroke version, but due to the difficulty of improving the volumetric efficiency (scavenging), it is used only for small passenger car engines and for very large truck engines.

1.3 Noise Sources

It is well known that the noise emitted from the engine itself (bare engine) is divided into two major categories by the nature of the source. One is combustion noise and the other is mechanical noise.

1.3.1 Combustion noise

Combustion noise is caused by the rapid pressure rise and high peak pressure in the combustion chamber during combustion. This occurs once per revolution per cylinder for the two stroke engine and once per two revolutions per cylinder for the four stroke engine. The fundamental frequency of combustion noise is:

$$f = \frac{Nn}{60Z}$$

where   N: engine rotation speed in rpm

           n: number of cylinders

           Z: for 2 stroke engine Z = 1

                   for 4 stroke engine Z = 2

Many studies have been done on combustion noise [7,8,9,10]. The following is a summary of those results from the point of view of frequency components. It is convenient here to consider the frequency spectra, because these spectra and frequency response of the surrounding structures determine the emitted engine noise.

The gasoline engine differs from the diesel engine in the cylinder pressure spectra, especially in the variation with change in applied load; but in general, the pressure decreases as frequency increases. This decay rate (slope of the envelope of all harmonics of fundamental frequency) is determined by the combustion type as shown in Table (1.1) [7]. Above 50% load, both the diesel engine and the gasoline engine show a more significant dependence of cylinder pressure spectra on speed than on load [11].

Since the maximum pressure components (at fundamental frequency) is virtually the same at all speeds, the speed dependence is considered to be a "shifting triangle" (the same spectrum is

- 13 -

ENGINE TYPE	DECAY RATE (dB/decade)
4 STROKE NA DIESEL	30
2 STROKE NA DIESEL	40
4 STROKE TC DIESEL	40
GASOLINE	50

NA : NATURALLY ASPIRATED

TC : TURBOCHARGED

TABLE 1.1 : DECAY RATE OF COMBUSTION NOISE
FOR VARIOUS ENGINE TYPES
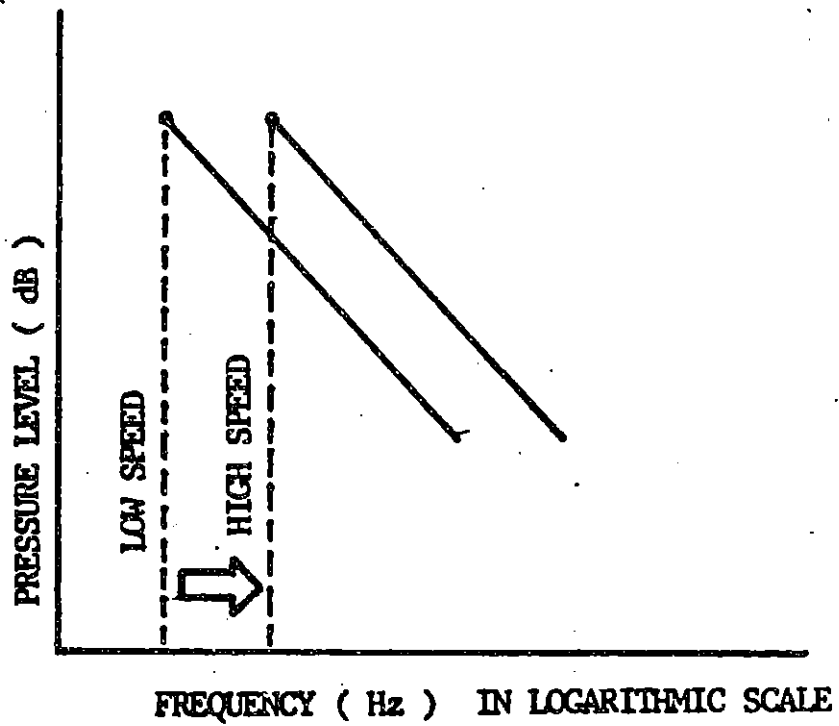
FIGURE 1.2 : SCHEMATIC REPRESENTATION OF

'' SHIFTING TRIANGLE ''

shifted with respect to the origin for various engine running speeds). It can be seen that the combustion noise is significant only in the lower frequency range because the cylinder pressure level becomes very small in the higher frequency range. For example, the fundamental frequency of the 4 cycle, 4 cylinder diesel engine with the maximum speed of 3800 rpm is 130 Hz and the pressure level is down 30 dB at 1300 Hz.

The magnitude of the combustion spectrum also varies with combustion type. The gasoline engine has a very smooth pressure rise in time (dp/dt). Due to the heterogeneous combustion, however, the diesel engine shows a steep dp/dt at the beginning of combustion. This steep rise, which is characteristic of the diesel engine, is improved by either retarding the combustion timing or turbocharging. This implies that the combustion noise plays an important role in different frequency ranges for each combustion type [7]. Combustion noise dominates below 1000 Hz for gasoline engine, below 2000 Hz for naturally aspirated diesel engine and below 1000 Hz for turbocharged diesel engine.

Methods of reducing the combustion noise vary for each engine model due to the fact that controlling the combustion noise means controlling the combustion itself. This directly affects the engine performance, including exhaust gas emissions, which is another important consideration for engine manufacturers. Therefore, reducing combustion noise by changing combustion involves trade-offs

with other factors for each particular engine model [8].

1.3.2 Mechanical noise

The so-called mechanical noise is the noise generated by various impacts between the engine parts. This noise source is more important in the higher frequency range rather than in the lower frequency range where combustion noise is important. There are lots of moving parts, for example, gears, valves, and rocker arms, piston and cylinder liner. Among these, piston slap noise, generated by the sudden impact of the piston to the cylinder wall, is considered to be predominant due to the higher amount of energy released.

Both experimental and theoretical studies have been carried out in this field [12-24]. The theoretical studies were concentrated in modeling the piston movement in the real operating cycle [12,13]. Some studies show very nice agreement between theoretical models and experiments. These models are usually very complicated and sometimes require empirical data taken from running engines to cover the unanalyzed portions, such as the compliance between the piston and cylinder liner due to the squeezing of the viscous oil film.

Figure 1.3 is the schematic representation of the piston movement. In this figure, the piston and the piston pin are shown

with an exaggerated clearance between them. The relationship between the piston pin hole and the piston pin tells whether the connecting rod is in a state of compression or tension.

In the compression stroke, the connecting rod pushes the piston upwards overcoming the gas force. Then the force acting on the piston has a lateral component in the direction shown (Fig. (1.3 (a))) and the piston slides upwards on the minor thrust side of the cylinder wall. As the piston moves through top dead center the gas forces dominate the inertial forces and keep the connecting rod in compression. Thus, as the crankpin passes through the cylinder centerline, the lateral component of force on the piston pin changes direction, causing the piston to accelerate through the clearance and slap against the major thrust side of the cylinder wall. (Fig. (1.3 (b))).

At bottom dead center the inertial force exerted by the piston on the connecting rod is in the same direction as the gas force and another slap, although much less severe, takes place as the crankpin once again passes through the cylinder centerline. (Fig. (1.3 (c))).

The simple model discussed above suggests that piston slap can occur at TDC and BDC [19]. The first one is considered predominant because it coincides with the combustion timing and the connecting rod is carrying the largest compressive load of the entire

(A)	(B)	(C)
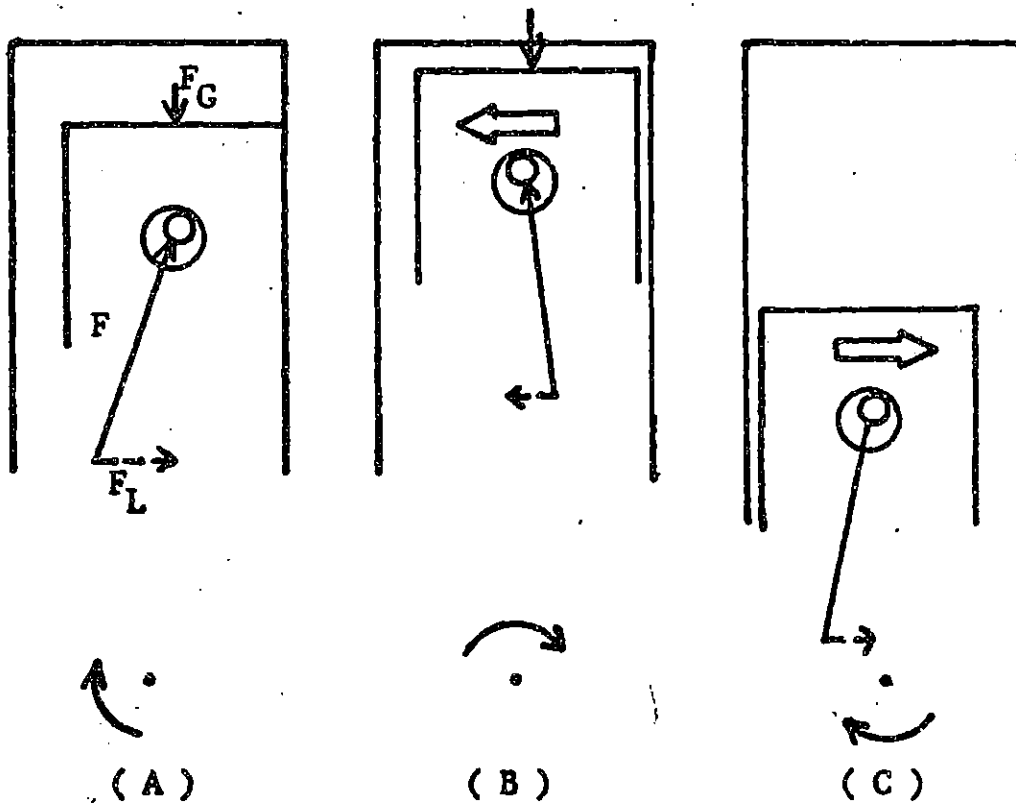
F   :   FORCE ACTING FROM THE CONNECTING ROD

F_L :   LATERAL FORCE ACTING ON THE PISTON

F_G :   GAS FORCE

⇐   :   DIRECTION IN WHICH PISTON IS ACCELERATED

↺   :   CRANK ROTATION

FIGURE 1.3   :   SCHEMATIC REPRESENTATION
OF THE PISTON MOVEMENT

    (A)   COMPRESSION STROKE

    (B)   AROUND TOP DEAD CENTER

    (C)   AROUND BOTTOM DEAD CENTER

cycle. A third possibilty is so-called mid-stroke slap, and rarely happens if the engine parts are properly designed and the engine is in proper operating condition.

Therefore, there are at least two piston slaps per revolution, but the major impact occurs at TDC before the power stroke. Neglecting all but this most significant impact, there will be one major piston slap per power stroke.

These simple models do not take into account other factors which may affect the piston motion such as:

. piston pin offset

. rocking motion of piston

. frictions at piston pin as well as piston's outer surface

. piston configuration, especially under operation

. pressure distribution around piston due to the squeezing motion of oil film

. compliance of cylinder liner wall

. cylinder liner deformation

These factors may cause a difference of about 20° crank angle between the simple model results and experimental results [13, 20].

Also, experimental data shows that side thrust force on the piston ranges up to 10^4N [17]. This is comparable with the

pressure force on the cylinder wall during combustion. This implies that piston slap as well as combustion, is a major noise source driving the cylinder wall.

Because of the nature of impact, the impacting force spectrum is considered to be band-limited white noise. Since no data taken from running engine was available to support this, the attempt was made to measure the frequency spectra of the impact on a non-running engine by impacting the connecting rod and measuring the acceleration inside the piston skirt. But this attempt was unsuccessful due to the lack of stiffness of the connecting rod. Therefore, instead of actual data, the assumption was made that the impact force spectrum is flat in the frequency range of 1000 Hz to 4000 Hz [21].

Finally, it is appropriate to mention the current techniques for piston slap noise reduction. The most effort has been focused on the piston. Lowering of noise levels was reported by E. A. Skobtsov, et. al. [22]. The techniques used were:

1. Reducing clearance between piston and cylinder liner
2. Wrapping the piston skirt with leather.

The first one is based on the assumption that the impacting energy increases with increase of lateral traveling distance of the piston. The second one is the attempt to add cushioning or compliant

material on the piston side.

Although the first technique may be considered to be the easiest technique to reduce the piston slap noise, it is difficult to achieve such a small clearance on the production line and maintain it during the whole operating life of the engine. If a smaller clearance than intended is obtained, cylinder liner wear, piston scuffing and in the worst case total engine failure by seizure of the piston in the cylinder may result.

Obviously, the second technique is not directly applicable because of its lack of durability, but a similar technique has been developed using a Teflon Pad on the thrust side of the piston [23].

Other newly developed techniques applicable to the piston are:

1. Thermal strut piston
2. Articulated piston
3. Piston pin offset

The thermal strut piston contains a steel strut inside the piston skirt. This strut controls the clearance between piston and cylinder wall during all operating conditions by controlling thermal expansion.

The articulated piston was developed to separate the two major roles of the piston; that of slider and vertical load carrier. The piston is divided into two parts connected to each other by the piston pin. The upper part (mainly ring lands) carries the combustion force and can rock back and forth. The lower part (skirt) slides up and down inside the cylinder. With this design it is easier to control the oil film thickness than when using a solid piston.

Piston pin offset is very commonly used. The basic idea is to shift the impact timing by setting the piston pin off the center line of the piston and thus off center in the cylinder. The amount of offset differs from engine to engine depending on their piston movement characteristics [24].

Up to this point current techniques to reduce piston slap noise have been examined. Generally the best way to control or reduce noise is to treat the source. But as long as the reciprocating engine is used, piston slap remains an unavoidable characteristic of the mechanism. More attention must be paid to reducing piston slap noise by modifying its transmission path. Very little is reported in this

area because few engine parts are involved and they are basic structural parts of the engine. This thesis has been directed towards clarifying the transmission path and finding methods for isolating piston slap noise.

CHAPTER 2

SOME MATHEMATICS

In this chapter, some computer programs and calculus used throughout this thesis are discussed. This chapter is divided into four parts as follows:

1. Data Taking Program

2. Data Reducing Technique

3. Analysis of Longitudinal Wave in Finite Bar

4. Reciprocity

2.1 Data Taking Program

The data taking program COHER was developed by R. DeJong and described in his doctoral thesis [25] and in documentation prepared at Acoustics and Vibration Laboratory at MIT.

The following operations are programmed on an Interdata Model M70. Two channels of analog data are simultaneously digitized by an A/D converter at a pre-specified sampling rate. The computer stores this data in an array and calculates two complex FFT. Assuming one channel is force and the other is acceleration, the computer then calculates, prints out, and punches on paper tape following six quantities:

f_j frequency in Hertz

PSD(F)   power spectral density of force $10 \log G_{FF}$

in dB re IN

PSD(A)   power spectral density of acceleration $10 \log$

G_{AA} in dB re $1m/s^2$

CPSD(AF)   cross sepctral density of force and acceleration

$10 \log |G_{AF}|$ in dB re $1N-m/s^2$

Φ_{AF} relative phase between acceleration and force

in degrees

γ^2 coherence.

These quantities are estimated from the Fast Fourier

Transform (FFT) as follows:

$$G_{XX}(f) = \lim_{T \to \infty} \frac{2}{T} E[|X(f,T)|^2]$$

where

$$X(f,T) = \int_0^T x(t) \, e^{-i2\pi ft} dt$$

is estimated as

$$\hat{G}_{XX}(f_j) = \frac{2}{Nh} |\hat{X}(f_j,T)|^2 = \frac{2h}{N}|X_j|^2$$

where

$$\hat{X}(f_j,T) = h \sum_{n=0}^{N-1} x(nh) \, e^{-i2\pi fnh}$$

and

$$X_j = \frac{1}{h} \hat{X}(f_j,T)$$

$$j = 0, 1, \ldots, \frac{N}{2} - 1$$

for cross spectral density

$$G_{YX}(f) = \lim_{T\to\infty} E[Y(f,T) \cdot X^*(f,T)]$$

is approximated by

$$\hat{G}_{YX}(f_j) = \frac{2}{Nh} Y_j X_j^*$$

Coherence is defined by

$$\gamma^2(f) = \frac{|G_{YX}(f)|^2}{G_{XX}(f)\ G_{YY}(f)}$$

and approximated by

$$\hat{\gamma}^2(f_j) = \frac{|<\hat{G}_{YX}(f_j)>|^2}{<\hat{G}_{XX}(f_j)><\hat{G}_{YY}(f_j)>}$$

where < > denotes an ensemble average. Averaging is used to reduce statistical error, and the number of sample spectra in each ensemble is specified for each run.

2.2 Data Reducing Technique

Two data reduction programs were created and used for processing the data. One program was used for reducing drive point data and the other for the transfer funation data.

- 27 -

2.2.1 Drive point data reduction program

The basic purpose of this program is to correct for the effects of mass and stiffness below the force gauge of the impedance head. The tip of the impedance head is modeled as a simple mass and spring. When using the impedance head to measure both force and acceleration, the measured data, F_0 and A_0, should be corrected to represent true force and acceleration at the drive point. Let F_1 and A_1 denote the true force and acceleration at the drive point.

$$F_1 = k(X_0 - X_1) = -\frac{k}{\omega^2}(A_0 - A_1)$$

$$F_1 = F_0 - mA_0$$

Using these two equations, A_1 and F_1 are derived from A_0, F_0 as follows:

$$F_1 = F_0 - mA_0$$

$$A_1 = (F_0 - mA_0)\frac{\omega^2}{k} + A_0$$

Then the drive point mobility and phase are derived from the following quantities which the computer calculates.

$$|Y(f_j)|^2 = \frac{1}{(2\pi f_j)^2} \cdot \frac{1}{(F_1 F_1^*)^2} [[|A|\{|F|\cos \phi_{AF} - m|A|\}$$

$$+ \frac{(2\pi f_j)^2}{k} F_1 F_1^*]^2 + |A|^2|F|^2 \sin^2 \phi_{AF}]$$

- 28 -
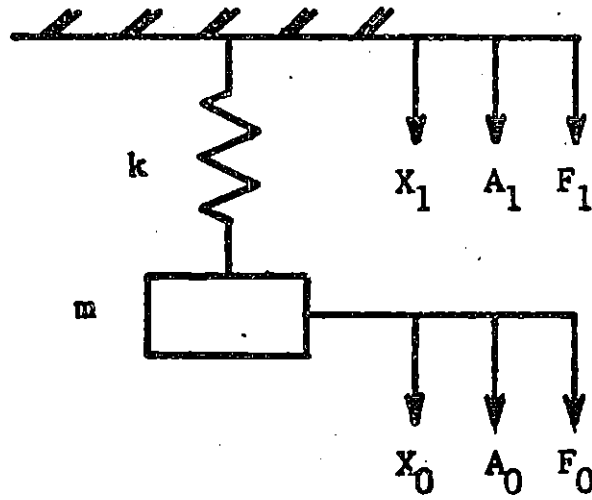
FIGURE 2.1 : LUMPED MODEL OF THE IMPEDANCE HEAD

$$\arg Y(f_j) = \arctan \frac{|A|\{|F|\cos\phi_{AF} - m|A|\} + \frac{\omega^2}{k} F_1 F_1^*}{|A| |F| \sin \phi_{AF}}$$

and

$$F_1 F_1^* = |F|^2 + m^2|A|^2 - 2m|A| |F|\cos\phi_{AF}$$

where $|A|$ and $|F|$ are calculated using CPSD(AF) and either PSD(A) or PSD(F). Although theoretically both quantities work, severe errors introduced by dynamic range limits of the instrumentation affect PSD(A) at resonance and PSD(F) at anti-resonance. Because the noise floor is the most serious limitation, the program compares the values of PSD(A) and PSD(F) and uses the larger quantity to calculate $|A|$ and $|F|$.

When PSD(F) is greater than PSD(A),

$$|F| = 10^{PSD(F)/20}$$

$$|A| = 10^{CPSD(AF)/10}/|F|$$

and when PSD(F) is less than PSD(A)

$$|A| = 10^{PSD(A)/20}$$

$$|F| = 10^{CPSD(AF)/10}/|A|$$

The values of m and k are 0.0215 kg and 1.2×10^9 N/m respectively as shown in Table 3.1.

2.2.2 Transfer Function Data Reduction Program

The second program was used to reduce the transfer function data. The transfer function used is mobility, i.e., velocity divided by force. The same consideration is used to obtain force and acceleration as stated above. Then using CPSD(AF) and either PSD(F) or PSD(A), the transfer mobility and phase are calculated as follows.

$$20 \log Y(f_j) = 2(CPSD(AF) - PSD(F)) - 20 \log (2\pi f_j)$$

or

$$20 \log Y(f_j) = 2(PSD(A) - CPSD(AF)) - 20 \log (2\pi f_j)$$

and

$$\arg (Y(f_j)) = \phi_{AF} - 90°$$

2.3 Longitudinal Wave Mobility of a Finite Bar

It was necessary to verify the experimental set up and data reduction technique. The longitudinal wave mobility of a finite bar was chosen because the theoretical mobility of that system could be easily calculated. The following is an analysis of that system and the calculated results are shown compared with the experimental results in Fig. (4.2) and Fig. (4.3).

The equation of motion for the longitudinal wave in a bar is:

$$\frac{\partial^2 u}{\partial t^2} = \frac{E}{\rho} \frac{\partial^2 u}{\partial x^2}$$

where $u = u(x,t)$ is the logitudinal deflection

E is the Young's modulus in N/m^2

ρ is the density of the material in kg/m^3

The boundary conditions for the free bar are:

$$\frac{\partial u}{\partial x} = 0 \text{ (no stress) at } x = L$$

$$\frac{\partial u}{\partial x} = -\frac{Fe^{-i\omega t}}{SE} \text{ (input stress) at } x = 0$$

where $Fe^{-i\omega t}$ is input force in N

S is cross sectional area in m^2

The complete solution of the equation is obtained by applying this boundary condition to the general solution,

$$u(x,t) = Be^{-i(\omega t - kx)} + Ce^{-i(\omega t + kx)}$$

where $k = \omega/c_L$ is the wavenumber

$c_L = \sqrt{E/\rho}$ is the longitudinal wave speed and

$$u(x,t) = \frac{-F \cos k (L-x)}{kSE \sin kL} e^{-i\omega t}$$

The small amount of internal damping of the bar was approximated by replacing the wave number k by the complex wave number k_d. The complex wave number k_d is defined as

$$k_d = k + i\beta$$

For the bar β can be related to the loss factor η,

$$\beta = \frac{1}{2} \eta k.$$

For $\beta^2 \ll 1$, the deflection $u(x,t)$ may be rewritten approximately as follows:

$$u(x,t) = \frac{-F\{\cos k(L-x) - i\beta(L-X) \sin k(L-X)\}e^{-i\omega t}}{(k+i\beta)SE(\sin k L + i\beta L \cos k L)} \quad .$$

The transfer mobility from $x = 0$ to any point in the bar is obtained by

$$Y = \frac{\frac{\partial u}{\partial t}}{Fe^{-i\omega t}}$$

$$= \frac{i\omega\{\cos k (L-X) - i \beta(L-X) \sin k (L-X)\}}{(k+i\beta)SE (\sin k L + i\beta L \cos k L)} \quad .$$

Then the drive point mobility at $x = 0$ is obtained as

$$Y = \frac{\omega\{\beta L \sin k L + i \cos k L\}}{(k+i\beta)SE(\sin k L + i\beta L \cos k L)}$$

and the transfer mobility from $x = 0$ to $x = L$ is obtained as

$$Y = \frac{i\omega}{(k+i\beta)SE(\sin kL + i\beta L \cos kL)}$$

These mobilities were expressed in terms of mobility magnitude and mobility phase using the following values:

$$S = 1.27 \times 10^{-4} m^2$$
$$E = 7.3 \times 10^{10} N/m^2$$
$$c_L = 5060 \text{ m/s}$$
$$\eta = 10^{-3}$$

2.4 Reciprocity

It is necessary to discuss reciprocity here because all the measurements carried out on the engine were the reciprocal of the desired transfer functions. The reciprocity statement says that for a system which has certain properties, the transfer function between two points on the system (ports) will be the same regardless of which is chosen as drive point and which is chosen as response point. (See Fig.(2.2).) In fact, the reciprocity statement remains unchanged even if V_1 and V_2 are generalized velocity variables with different units (e.g. translation and rotation) as long as the product $V_1 F_1$ and the product $V_2 F_2$ have units of power.

Reciprocity applies to any system which satisfies the following requirement [26]:

1. the system is linear
2. no element of the system can generate energy
3. the elements neighboring each other can play the reversal role in transferring force and resultant motion.

The engine components should satisfy those requirements.
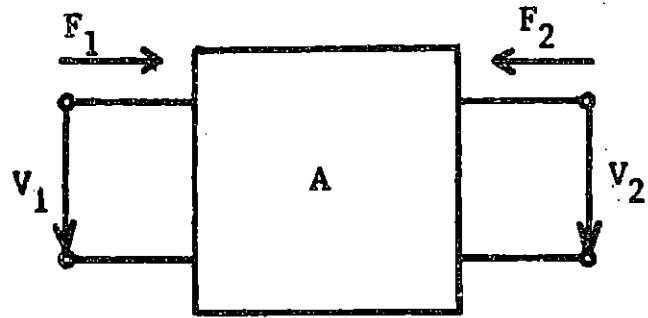
IF SYSTEM A SATISFIES RECIPROCITY ,

$$\left.\frac{V_2}{F_1}\right|_{F_2=0} = \left.\frac{V_1}{F_2}\right|_{F_1=0}$$

FIGURE 2.2 : SCHEMATIC REPRESENTATION OF RECIPROCITY

CHAPTER 3

INSTRUMENTATION

3.1 Test Set-Up

Fig. (3.1) shows the test set-up with which verification tests and experiments on the engine were carried.

The B&K 1402 White Noise Generator and the B&K 1612S2 Spectrum Shaper were used to generate an input spectrum of shaped broad band noise to the shaker in order to get as much as possible of both the force and the acceleration within the dynamic range of the instrumentation. A relatively large difference in sensitivity between a 2gm B&K 4344 accelerometer and force gauge of the impedance head compensated for by using an ITHACO 432 preamplifier in both channels and by applying a signal as larger as possible to the shaker.

In order to preserve the relative phase between the two channels, K&H 3550 band-pass filters were used for both channels and the whole system was checked with a phase-meter to verify the phase. The band-pass filters were set to pass 200-5000 Hz. The sampling rate was set to 2.5 times the 5000 Hz high frequency roll off to avoid an aliasing error.
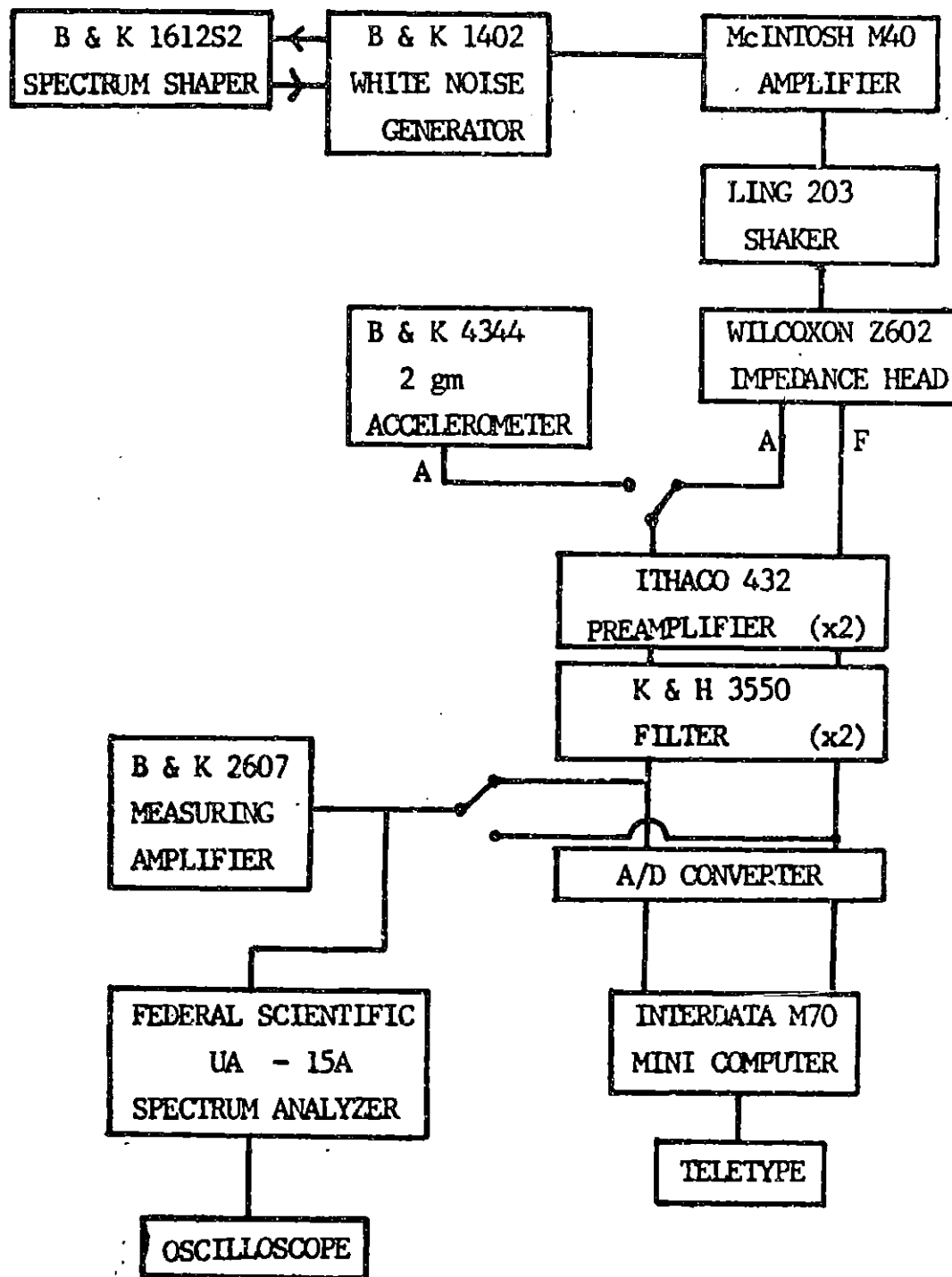
```
┌─────────────────────┐      ┌─────────────────────┐          ┌─────────────────────┐
│   B & K 1612S2      │ ◄─── │    B & K 1402       │          │   McINTOSH M40      │
│  SPECTRUM SHAPER    │ ───► │    WHITE NOISE      │──────────│    AMPLIFIER        │
│                     │      │    GENERATOR        │          │                     │
└─────────────────────┘      └─────────────────────┘          └─────────────────────┘
                                                                         │
                                                              ┌─────────────────────┐
                                                              │    LING 203         │
                                                              │    SHAKER           │
                                                              └─────────────────────┘
                                                                         │
                     ┌─────────────────────┐                  ┌─────────────────────┐
                     │    B & K 4344       │                  │  WILCOXON Z602      │
                     │    2 gm             │                  │  IMPEDANCE HEAD     │
                     │   ACCELEROMETER     │                  └─────────────────────┘
                     └─────────────────────┘                        A │    │ F
                          A │
                                                         ┌─────────────────────────┐
                                                         │    ITHACO 432           │
                                                         │  PREAMPLIFIER    (x2)   │
                                                         └─────────────────────────┘
                                                         ┌─────────────────────────┐
     ┌─────────────────────┐                             │    K & H 3550           │
     │    B & K 2607       │                             │    FILTER        (x2)   │
     │    MEASURING        │                             └─────────────────────────┘
     │    AMPLIFIER        │                                         │
     └─────────────────────┘                             ┌─────────────────────────┐
              │                                           │    A/D CONVERTER        │
              │                                           └─────────────────────────┘
     ┌─────────────────────┐                                        │
     │ FEDERAL SCIENTIFIC  │                             ┌─────────────────────────┐
     │    UA - 15A         │                             │   INTERDATA M70         │
     │  SPECTRUM ANALYZER  │                             │   MINI COMPUTER         │
     └─────────────────────┘                             └─────────────────────────┘
              │                                                      │
     ┌─────────────────────┐                             ┌─────────────────────────┐
     │    OSCILLOSCOPE     │                             │      TELETYPE           │
     └─────────────────────┘                             └─────────────────────────┘
```

FIGURE 3.1 :   EXPERIMENTAL SET-UP

- 38 -

Due to the input voltage limitation of the A/D converter, a B&K 2607 measuring amplifier was used to monitor the input, and the input signal was controlled so as to get voltage peaks which only occasionally exceeded 5V.

The output spectrum from both channels were monitored by spectrum analyzer and input spectrum was controlled by spectrum shaping panel as mentioned above.

The dynamic range of this system was estimated to be 50-60 dB for the mobility measurement [25]. The normalized standard error of this system is:

$$error = \sqrt{1/N}$$

where N is the number of data sets used for averaging.

Throughout this thesis, averaging number of 800 was used, then normalized standard error of the result was

$$error = \sqrt{1/800} = 0.0354 = 3.54\%$$
$$(20 \log 1.0354 = 0.3 \text{ dB}).$$

This measuring system was calibrated by the method stated in the next section.

3.2 System Calibration

Calibrations were done for the measuring system, and the

measuring transducers.

3.2.1 Transducer calibration

The transducer calibrations were done by the following

procedure:

(a) Calibrate 2 gm accelerometer using General Radio GR/1557-A

Acceleration Calibrator, which gives 1 g rms at 100 Hz.

(b) Calibrate the accelerometer of the impedance head by shaking

it with the 2 gm accelerometer attached (at 100 Hz).

(c) Attach the impedance head to the mass and shake at 100 Hz to

calibrate the force gauge of the impedance head.

The force gauge was calibrated as follows:

From the relationship:

$F = (m + m') A$

m: Mass attached in kg

m': Mass below the impedance head in kg

A: Acceleration in m/s^2

$F_G = F \cdot F_S$

F_G: Voltage gain of force in V

F_S: Sensitivity of impedance head in V/N

Then the force sensitivity is obtained as:

$F_S = F_G/F$

$= F_G/(m + m')A$

- 40 -

This calibration was done for each transducer with the measured signal passing through all the cables and instruments used for that channel. But the calibration data shows a large difference in sensitivity between force gauge and accelerometer, which implied the necessity of large amplification for the acceleration channel in order to use the entire dynamic range of the A/D converter. Therefore, the entire system including the A/D converter was calibrated as described in the next section.

3.2.2 System calibration

This calibration was done with the same set-up as testing and the procedure was as follows.

(a) Calibrate the accelerometer. (Same as Transducer Calibration).
(b) Calibrate the impedance head force gauge by shaking with broad band noise. The outputs were processed by using COHER program. The relationship between the output voltage and sensitivity is as follows.

$$F = F_G/F_S$$

F_G: Voltage gain of force in V

F_S: Sensitivity of impedance head in V/N

Then if F_S at a level of 0 dB is input to the computer program, the data obtained by COHER will be 20 log F_G. Using the relation-

ship F = mA, the force sensitivity is calculated by

$$20 \log F = 20 \log F_G - 20 \log F_S$$

$$
\begin{aligned}
20 \log F_S &= 20 \log F_G - 20 \log F \\
&= 20 \log F_G - 20 \, (\log(m+m') + \log A) \\
&= 2 \, (CPSD(AF) - PSD(A)) - 20 \log(m+m')
\end{aligned}
$$

Where CPSD(AF) and PSD(A) represent cross spectral density of acceleration and force, and power spectral density of acceleration respectively. (See Section 2.1, "Data Taking Program".)

(c) Calibration of the impedance head accelerometer used the same technique as (b). In this case, if the accelerometer sensitivity A_S is set to 0 dB, the output obtained will be $20 \log A_G$. Then sensitivity A_S is calculated by:

$$A = A_G/A_S$$

$$
\begin{aligned}
20 \log A_S &= 20 \log A_G - 20 \log A \\
&= 20 \log A_G - 20 \log F/(m+m') \\
&= 20 \log A_G - 20 \log F + 20 \log \, (m+m') \\
&= 2 \, (PSD(A) - CPSD(AF)) + 20 \log \, (m+m')
\end{aligned}
$$

0.0215 kg is used for the mass below the force gauge of impedance head according to the calibration data.

(d) Due to using an average value for a wide frequency range for force and acceleration sensitivity, it was necessary to check for accuracy once again. This was done by shaking the impedance head without the 2 gm accelerometer.

The data was taken with sampling rate of 12,500 samples/sec, 512 samples per channel and 800 averages. The result shows less than 0.2 dB difference in magnitude and less than 3 degrees variation in phase in the frequency range 500 - 5000 Hz.

3.3 Calibration Results

The calibration data are shown in Table (3.1), compared with manufacturer's data. The data taken using the two calibration techniques mentioned above show good agreement with each other and with the manufacturer's data. The values which were measured for impedance head by previous work were used in this thesis [25]. These mass and stiffness corrections are important to obtain accurate values at the attaching point. (See Section 2.2.1: "Drive Point Data Reduction Program").

SENSITIVITIES OF THE TRANSDUCERS

TRANSDUCER		UNIT	CALIBRATION DATA		MANUFACTURER'S DATA
			(1)	(2)	
2gm ACCELEROMETER B & K 4344 SERIAL NO. 243553		dB re $1V/1m/s^2$	−75.2	−75.2	−74.8
IMPEDANCE HEAD WILCOXON Z602 SERIAL NO. 252	FORCE GAUGE	dB re 1V/1N	−10.6	−10.4	−10.4
	ACCELEROMETER	dB re $1V/1m/s^2$	−53.0	−53.6	−53.3

MASS AND STIFFNESS BELOW FORCE GAUGE

WILCOXON Z602 IMPEDANCE HEAD		UNIT	CALIBRATION DATA	MANUFACTURER'S DATA
	MASS	kg	0.0215	0.021
	STIFFNESS	N/m	1.2×10^9	1.05×10^9

TABLE 3.1 : CALIBRATION DATA

CHAPTER 4

EXPERIMENTS ON THE ENGINE AND ANALYSIS OF TEST RESULTS

The two engines were tested using the experimental set-up shown in Fig. (3.1). The impendance head was epoxied on the measuring points shown in Fig. (4.1). The impedance head is connected to the shaker by a flexible shaft to minimize bending loads and avoid failure of the shaker due to the misalignment between the shaker and the impedance head. The shaker was mounted on a foam pad so as to get a large enough load capacity to shake the large structure. The accelerometer was attached on the cylinder liner wall using beeswax. The nomenclature of the measuring points is as follows:
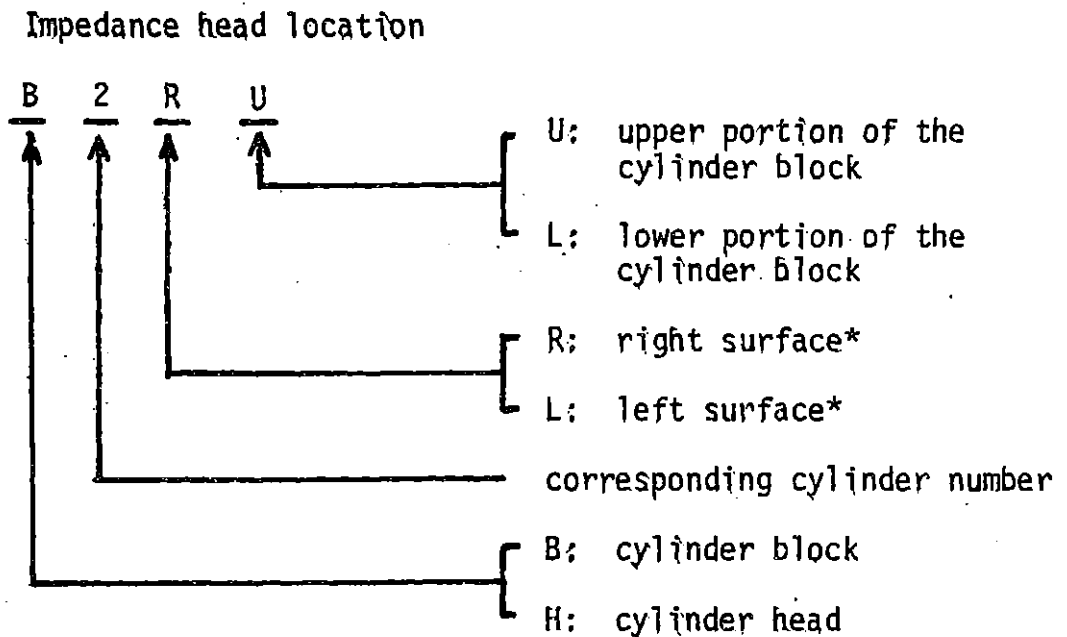
Impedance head location

```
B   2   R   U
─   ─   ─   ─        ┌  U:  upper portion of the
↑   ↑   ↑   ↑        │      cylinder block
                     └  L:  lower portion of the
                            cylinder block

                     ┌  R:  right surface*
                     └  L:  left surface*

                        corresponding cylinder number

                     ┌  B:  cylinder block
                     └  H:  cylinder head
```

*Right and left of engine is defined by looking at the engine behind the flywheel housing.

B3RU   B2RU   H2R   B1RU

B1LU   B2LU   B3LU

B2RL   B1RL

1   2   3   4

B2LL

CYLINDER CENTER LINES
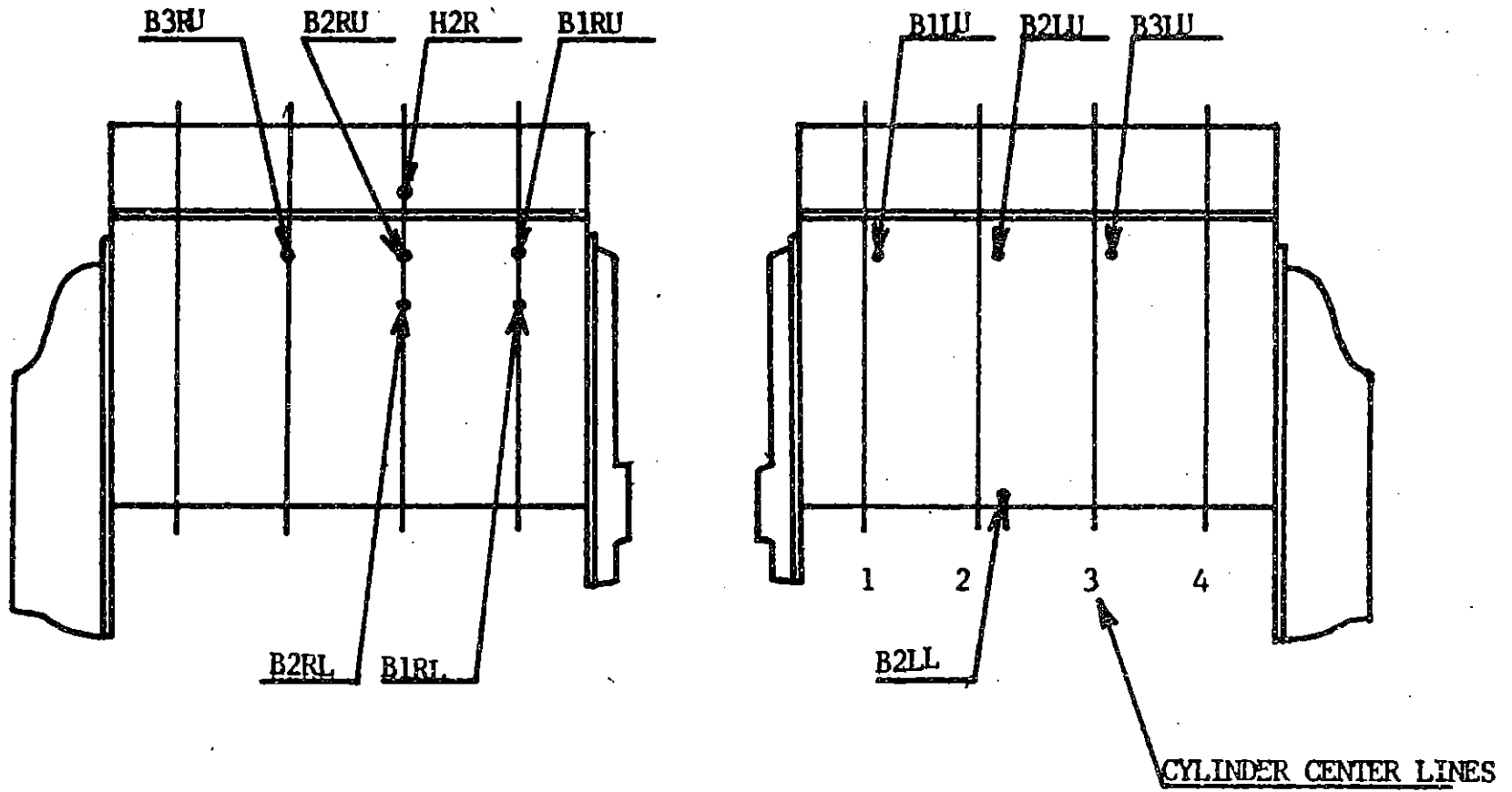
FIGURE 4.1 :   MEASURING POINTS FOR ENGINE TEST

Accelerometer location

<u>2</u> <u>R</u> <u>50</u>

                  distance in mm from the
                  top surface of the cylinder
                  block

                  R: cylinder right wall*

                  L: cylinder left wall*

                  cylinder number
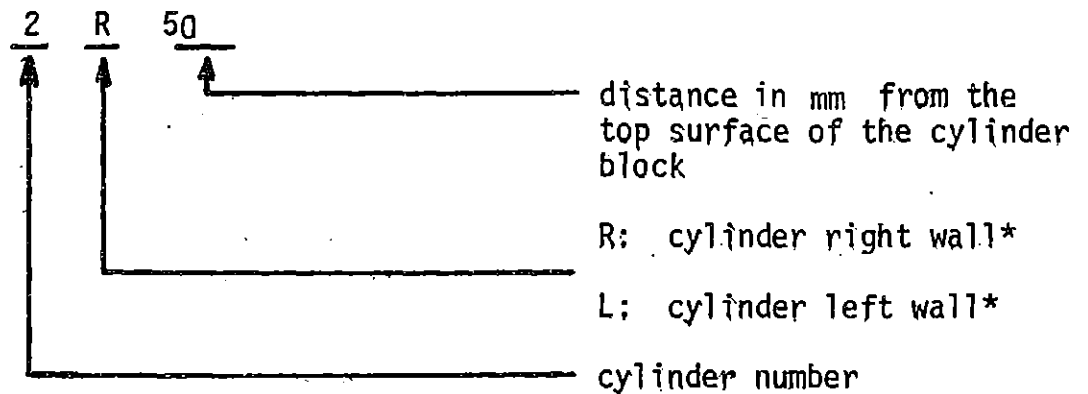
*Right and left of engine is defined by looking at the engine behind

the flywheel housing.

4.1   Verification test

The verification test was done to verify the measuring

system and data processing method. An aluminum bar was chosen as a

simple structure whose mobility is analytically determined as

described in Section 2.3. The material properties of the

aluminum bar were determined by measuring the lowest resonance

frequency. Then Young's Modulus was calculated by using the

following equation:

$$c_L = \sqrt{E/\rho}.$$

Those properties necessary to calculate the mobilities are listed

below.

Length (1)	:	0.55 m
Cross Sectional Area (S)	:	1.27×10^{-4} m^2
Mass (m)	:	0.2 kg
Density (ρ = m/S1)	:	2850 kg/m^3
Wave Speed (c_L)	:	5060 m/s
Young's Modulus (E)	:	7.3×10^{10} N/m^2 .

This aluminum bar was carefully mounted on a flat foam pad. The impedance head was bolted by short and rigid attachment to the shaker and the impedance head is bolted on end of the test piece. To get the pure longitudinal wave, an accelerometer was attached on the bar perpendicular to its longitudinal axis. The best impedance head alignment was determined by minimizing the accelerometer output in the frequency range of interest.

This aluminum bar was shaken by longitudinal force input and two measurements were done to obtain the drive point mobility and transfer mobility from one end to the other. The drive point mobility was calculated from force and acceleration output from the impedance head using mass and spring correction technique described in Section 2.2.1.

The transfer mobility was calculated from both force and acceleration outputs from the impedance head and from acceleration

measured by the 2gm accelerometer attached to the other end of the bar. Because the test set-up had only two channels, the test was carried out as follows.

(a) The spectrum shaper was set to get nice outputs for both the force and the acceleration channels. The amplifier and spectrum shaper were kept at that setting and acceleration and force signals from the impedance head were measured simultaneously.

(b) Keeping the settings of the spectrum shaper and amplifier, the acceleration channel was changed from impedance head to 2gm accelerometer, and the far end acceleration signal was measured simultaneously with the force signal.

(c) Data was reduced by the program which consists both programs described in Section 2.2.1 and Section 2.2.2 based on the assumption that the force input was random with respect to time. Prior to reducing the data, PSD(F) was checked by comparing both outputs obtained by (a) and (b). Their differences were no more than 0.2 dB in the entire frequency range of interest.

Analytically calculated mobilities are compared with measured data, Fig. (4.2) and Fig. (4.3) as drive point mobility and transfer

FIGURE 4.2 : DRIVE POINT MOBILITY OF AN ALUMINUM BAR
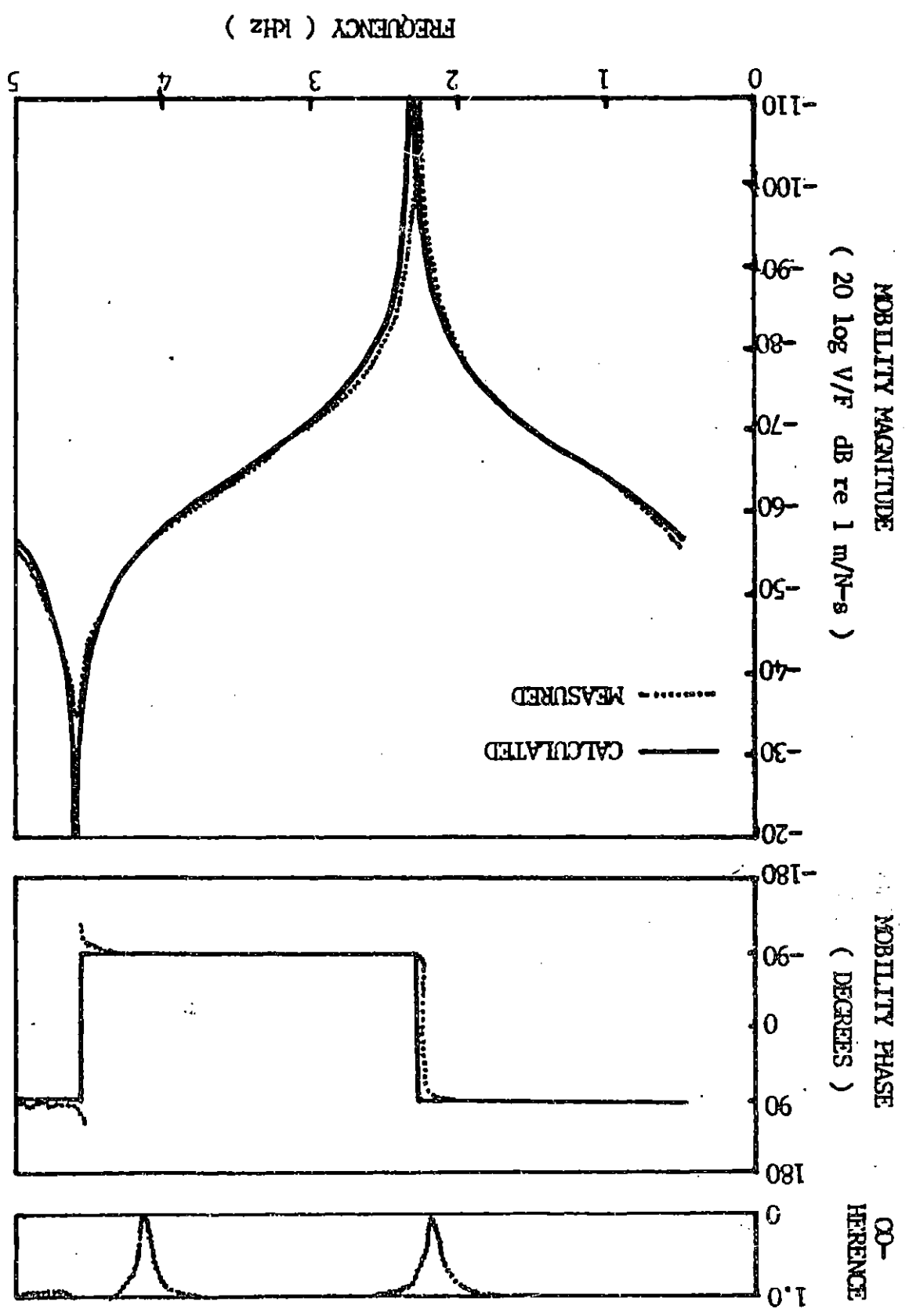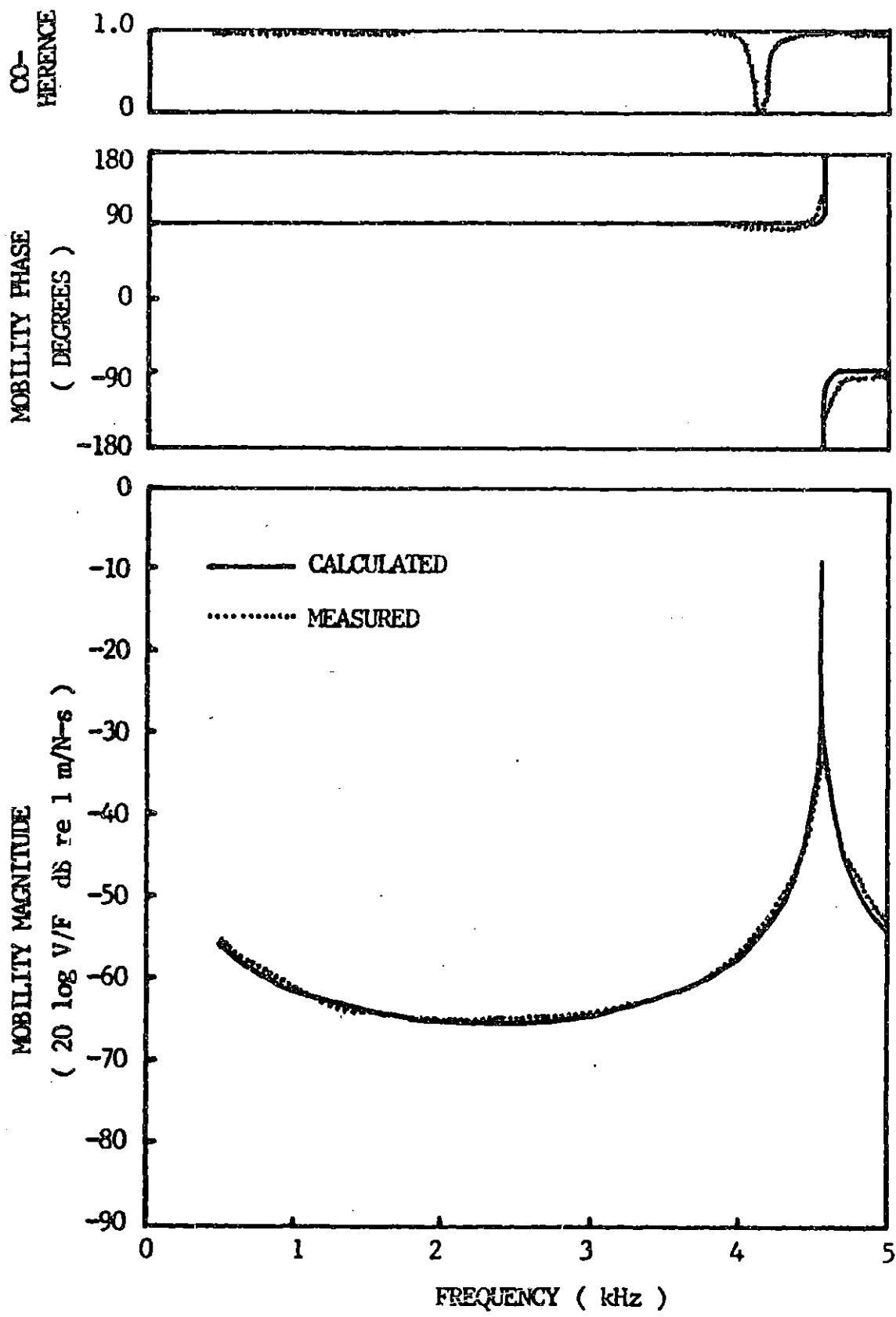
FIGURE 4.3 : TRANSFER MOBILITY OF AN ALUMINUM BAR
(FROM ONE END TO THE OTHER END)

mobility, respectively. The test results show nice agreement with the ones derived analytically. This verifies both of the data taking technique and data reducing technique.

4.2   Reciprocal Measurement

The reciprocal measurement was needed to verify reciprocity for the engine. Because the shaker suitable for shaking as large a mass as the engine block was too large to put into the cylinder, the measurements were carried out reciprocally. The force was applied to the outer surface and the vibration inside the cylinder was measured rather than applying force to the cylinder liner wall and measuring vibration on the cylinder block outer surface as is the case for piston slap.

This reciprocity verification measurement was done between two surface points. The locations for the impedance head and accelerometer were chosen on the right surface of the cylinder block (measuring points B1RU and B2RU), and the results are shown in Fig. (4.4).

In this figure, the mobility magnitudes show good agreement except in the frequency range between 2 and 3 kHz and in regions coherence drops. Outside of those frequency bands, resonances and anti-resonances coincide and the magnitudes are nearly the same.

The mobility phases are quite similar to each other except for in the region where coherence is low. But even in the 2-3 kHz frequency range, the mobility phases are nearly the same.

The difference in the mobility magnitude in the particular frequency range (it is worthwhile to discuss this here because this frequency range is the most important for the transmission of the piston slap noise) is considered to be the result of the difference in input impedance of each shaking point. The input impedance varies from place to place as well as with frequency. If the input impedance is low at a particular point, the actual force input is smaller than that which is obtained as the computer output and the corresponding acceleration response is small, which results in low coherence as well as low mobility magnitude.

The same reciprocal measurements were repeated three times between different shaker and accelerometer locations on the outer surface of the engine. All those results showed the same tendency described above, but in different frequency ranges which indicate that the difference in mobility magnitude is due to the different input impedances at each shaking point. The reciprocal measurements licate that the reciprocity assumption is valid in the frequency range of interest as long as the measurements show good coherence.
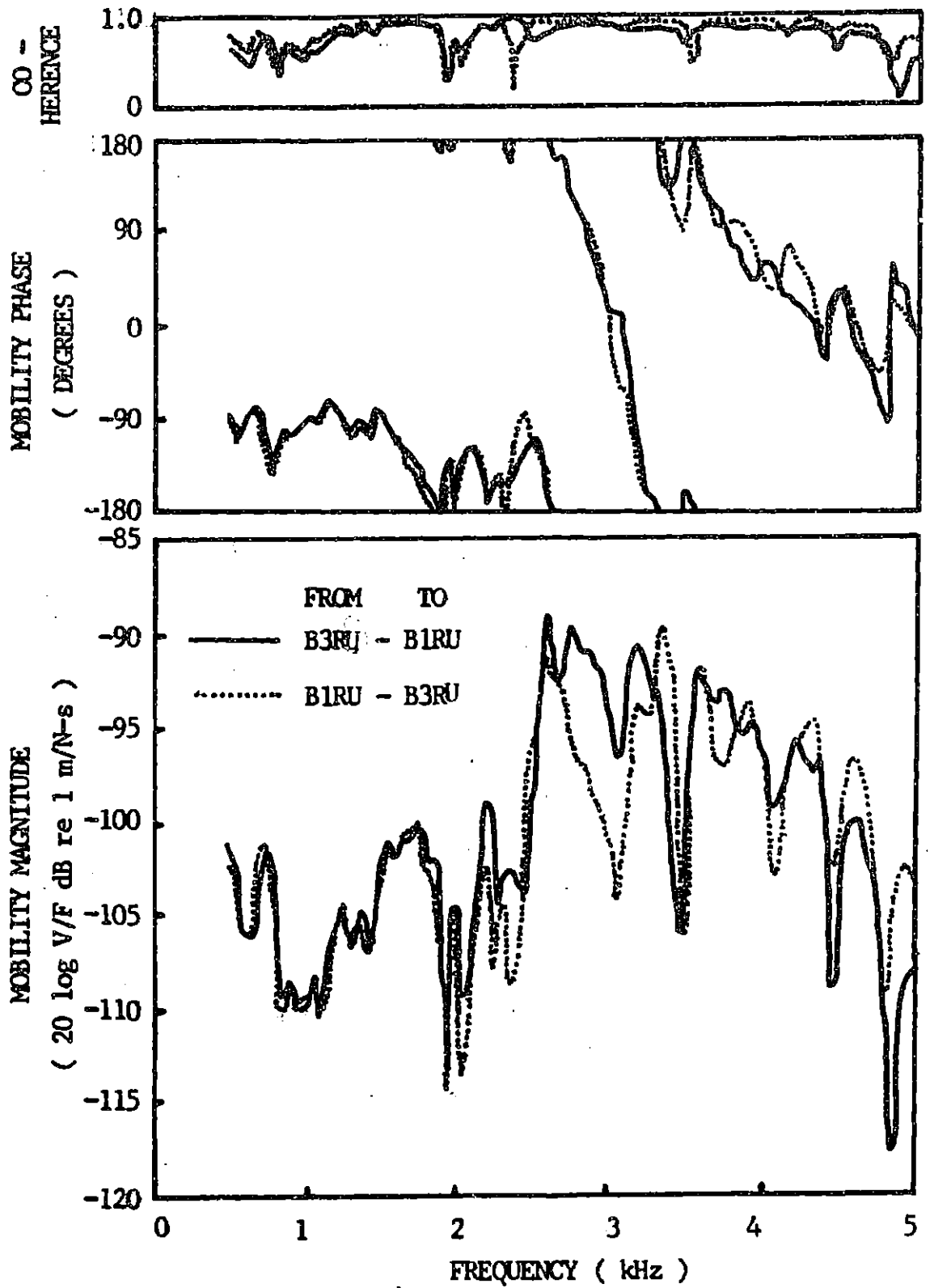
FIGURE 4.4 : RECIPROCAL MEASUREMENTS

BETWEEN TWO SURFACE POINTS

Also Fig. (4.4) shows that coherence is an indication of the accuracy of the measurement. All the experiments were checked first by examining the coherence obtained. Typical values of the coherence obtained by engine tests were above 0.90 in the frequency range between 1500 Hz and 4500 Hz and above 0.95 in the frequency range between 2000 Hz and 3500 Hz except for at resonances and anti-resonances.
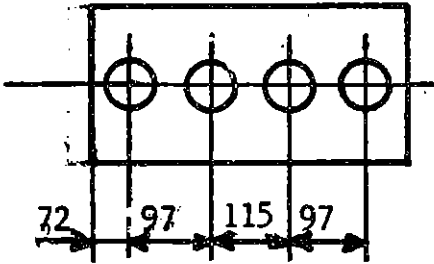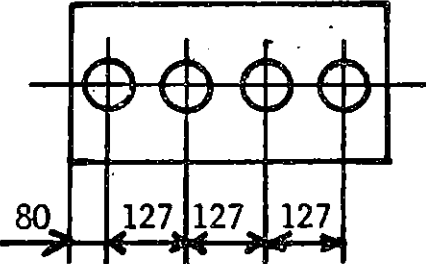
4.3 Engine Test

In this chapter, the results of various transfer mobility measurements are presented and compared to clarify the transmission path of the piston slap noise.

4.3.1 Engines used for the experiments

The transfer mobility measurements were carried out on the two engines. The specifications for those engines are listed in Table (4.1). Both engines were mounted on a rigid steel frame using resilient mountings which were considerably softer than the engine structure itself.

4.3.2 Preliminary Test

The Isuzu engine was tested in various conditions to eliminate the engine parts which played a minor role in transferring the piston slap noise to decide the final configuration for

MAKE AND MODEL	ISUZU C240	JOHN DEERE 4219 DF
CYLINDER	4 , IN LINE	4 , IN LINE
BORE	86 mm	102 mm
STROKE	102 mm	110 mm
DISPLACEMENT	2369 cc	3589 cc
HORSEPOWER	74 PS / 3800 rpm (MAXIMUM)	70 HP / 2500 rpm (RATED)
WEIGHT	200 kg	383 kg
OVERALL SIZE	.69 x .60 x .66 m	.5 x .81 x .83 m
CYLINDER BLOCK	CAST IRON	CAST IRON
CAM LOCATION	RIGHT MIDDLE	RIGHT MIDDLE
CYLINDER LINER	DRY	WET
SLEEVE OR LINER THICKNESS	1 mm	8 mm
CYLINDER BLOCK OVERALL SIZE (1) (2)	.165 .27 x .445 x .27 m	.235 .35 x .54 x .415 m

CYLINDER

ARRANGEMENT

(1) AT THE UPPER DECK

(2) AT THE LOWER DECK

TABLE   4.1   :   ENGINE SPECIFICATIONS

testing the engine.

At first, the major peripheral parts, such as alternator, starting motor and injection pump were removed on the assumption that, since those parts were installed on the ends of the cylinder block, they should not make any difference in the transmission path of piston slap noise. Then the measuring point near the crankcase joint B2LL was chosen to monitor the effect of the presence of crankcase, oil pan and main rotating system.

Because the oil pan is considered to be the most important among the engine covers which are vibrated by the structural parts of the engine, and particularly for this Isuzu engine, whose cylinder block is separated into cylinder block and oil pan-crankcase assembly by the horizontal plane at the crank shaft center, it was considered appropriate to monitor the transfer mobility at the oil pan joint to see whether lateral vibration was transmitted through the piston-connecting rod-crankshaft path.

A considerable change was observed in the transfer mobility magnitude between B2LL and 2L80 (No. 2 cylinder) after removing the oil pan and crankcase. Most of the resonances and anti-resonances coincided but a much higher (10 dB) magnitude was observed after removing the oil pan-crankcase assembly. This appeared to be the effect of removing a substantial amount of damping.

The similarity of the mobility phase supports this conclusion and the same effect, the loss of damping, was observed in the drive point mobility. This effect was expected and the experiments were carried out without the oilpan-crankcase assembly for an easy access since there was no fundamental change in the transfer mobility.

By removing the piston and connecting rod assembly from the No. 2 cylinder and measuring the transfer mobility to 2L14, a similar magnitude was obtained except in the region around 3.5 kHz where much higher magnitude was observed after removing the assembly. In addition, there were small decreases in the resonant and anti-resonant frequencies.

During this test it was assumed that the all bearing joints were well lubricated and that there was no metal to metal contact. But it was difficult to assure this, and because removing the piston-connecting rod assembly affected the transfer mobility as a reduction of the mass of the system, all the piston-connecting rod assemblies and main bearings were removed from the engine. The crankshaft was supported by the front and rear seals. All the measurements were done in this condition. The test results shown in Section 4.3.3 through Section 4.3.6 are measured on the Isuzu engine.

For the John Deere engine, tests were carried out on the cylinder block assembly including the flywheel housing and front

cover. Measurement points were chosen in order to make specific comparisons with the Isuzu engine. The measurements were done on the upper portion of the cylinder block surface (corresponding to B2RU of the Isuzu engine.) For reasons discussed later (Section 5.1.1), the lower portion of the cylinder block surface was considered to be less significant on the John Deere than on the Isuzu. As a result, fewer measurements were made on the John Deere engine.

4.3.3 Effect of the presence of cooling water

Although the experiments carried out were static and several parts were disassembled, it was worthwhile to attempt to approximate the real running condition.

Both engines tested employ water cooling so that each cylinder is surrounded by cooling water and it is possible to consider one transfer path as cylinder liner wall through cooling water to cylinder block surface. Therefore, comparison was made between the presence and the absence of cooling water in the Isuzu engine.

The test results are shown in Fig. (4.5) through Fig. (4.7). These figures indicate that the major transfer path of the vibrational energy from the inside wall of the cylinder is through the structural parts of the engine. The cooling water contributes mainly as a mass effect for the major transfer path (B2LU-2R50), and as additional damping for the minor transfer path (B2LU-4L150). (The major and
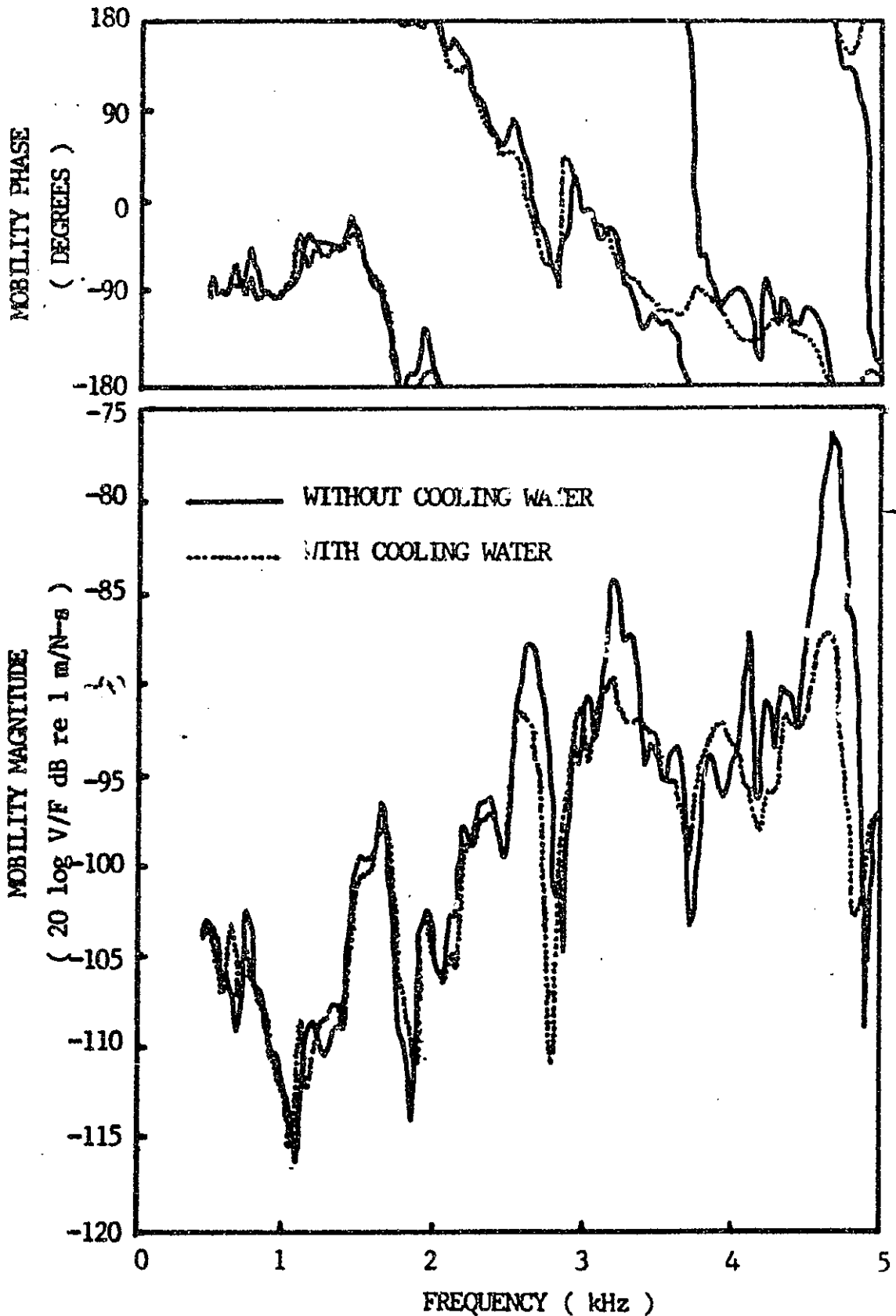
FIGURE 4.5 : EFFECT OF THE PRESENCE OF COOLING WATER ON THE
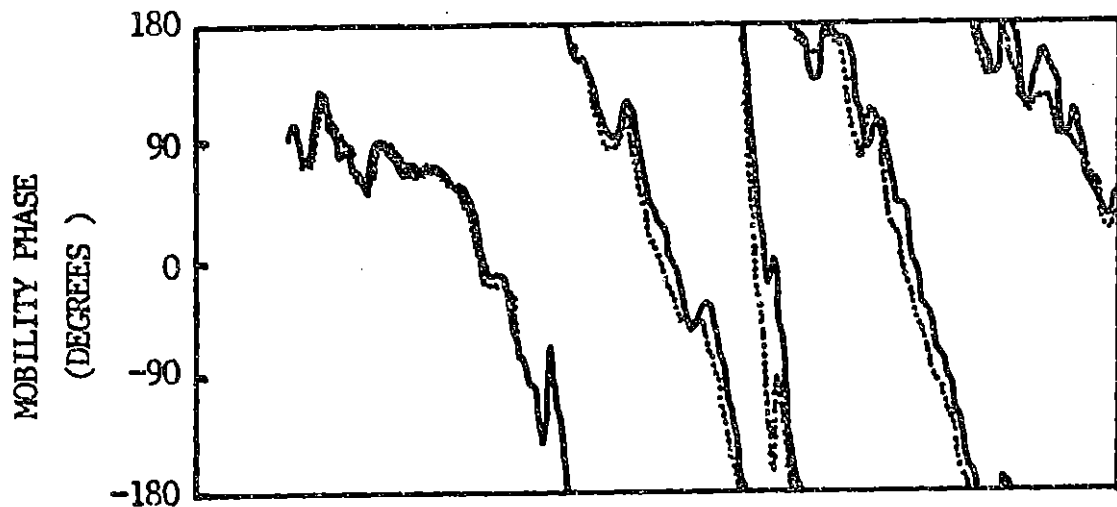TRANSFER MOBILITY (B2LU – 1R50)
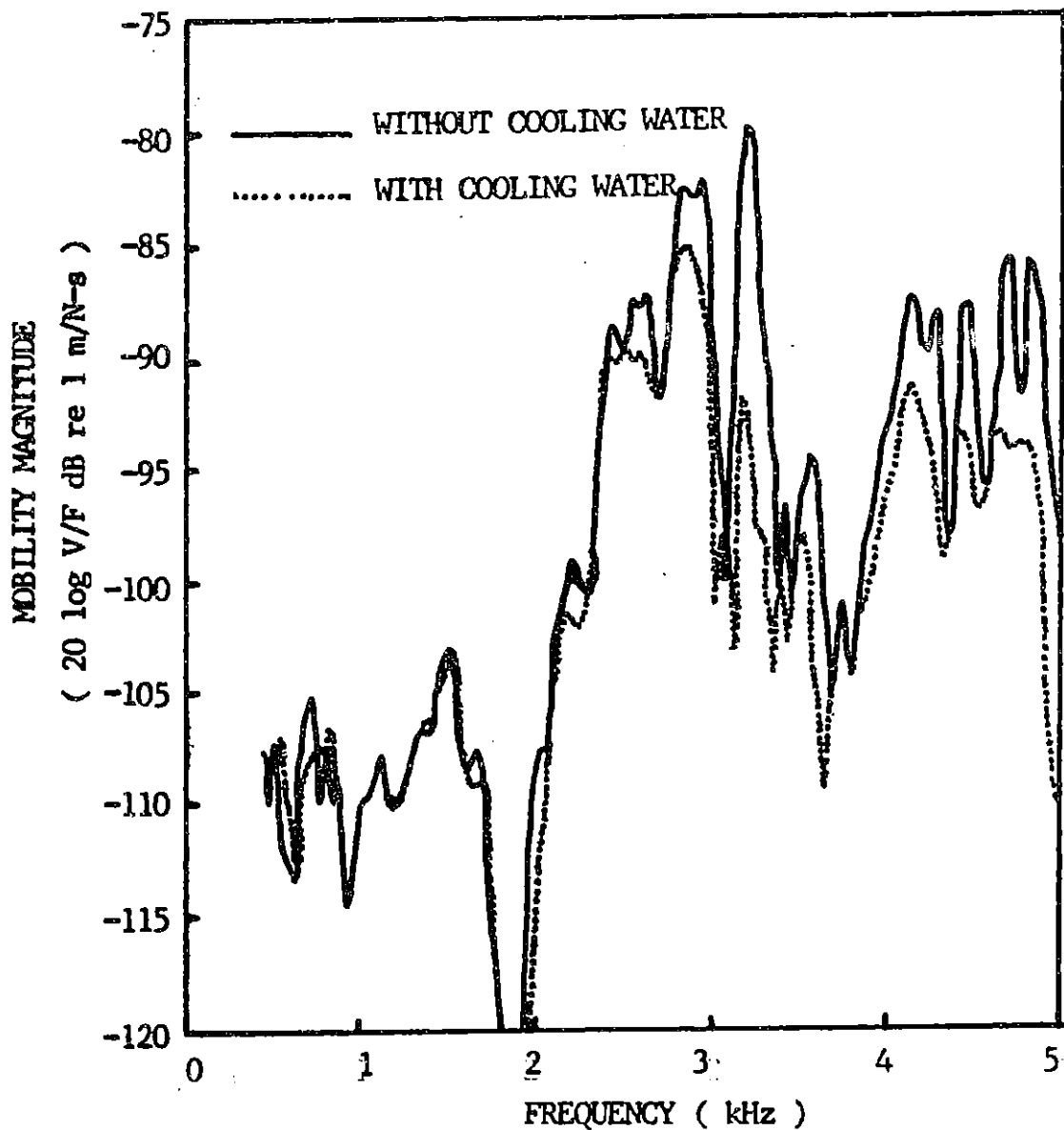
FIGURE 4.6 : EFFECT OF THE PRESENCE OF COOLING WATER ON THE
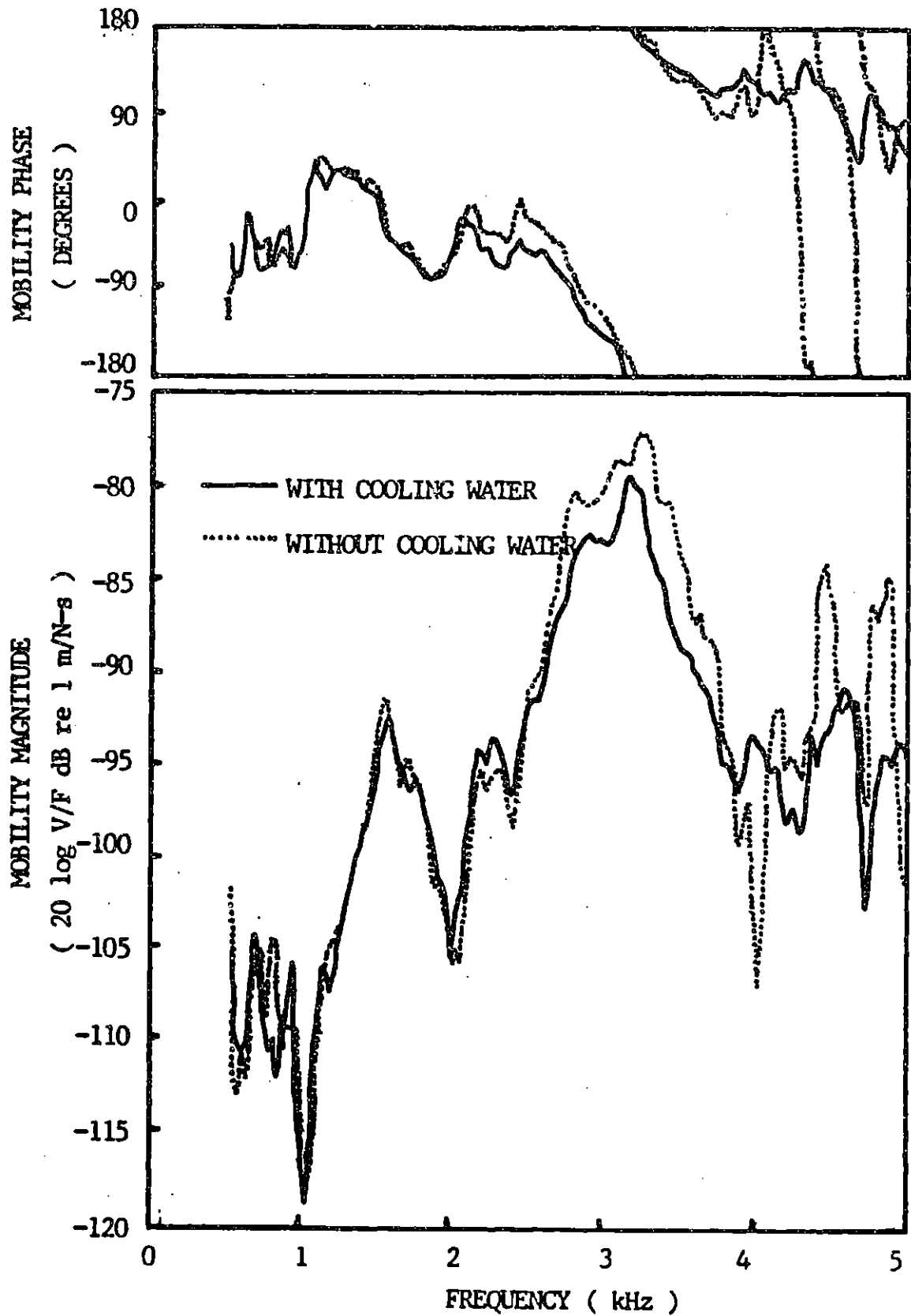TRANSFER MOBILITY (B2LU – 4L150)

FIGURE 4.7 : EFFECT OF THE PRESENCE OF COOLING WATER ON THE
TRANSFER MOBILITY (B2LU – 2R50)

minor transfer paths are discussed in Section 4.3.6).

The experiments were carried out either with or without cooling water present according to which condition was most convenient. The test results shown in this thesis were all done with water present unless otherwise specified.

4.3.4 Effect of the presence of the cylinder head

Figures (4.8) and (4.9) show the effect of the presence of the cylinder head on different transmission paths. Two different transmission paths were chosen to compare the effect. One was measured on cylinder No. 2 by shaking at the lower portion of cylinder block left surface, the other was measured on cylinder No. 3 by shaking at the upper portion of the cylinder block right surface. In both cases an accelerometer was attached on the corresponding cylinder liner right wall 50 mm from the top surface of the cylinder block. The schematic drawing of the cross-sectional view along the cylinder center line is shown in each figure.

The upper and lower transmission paths were compared on two different cylinders by assuming the cylinder block structure was symmetric about the junction between cylinders 2 and 3. This assumption was verified by measuring the transfer mobility for cylinders No. 2 and No. 3 as shown in Fig. (4.10).
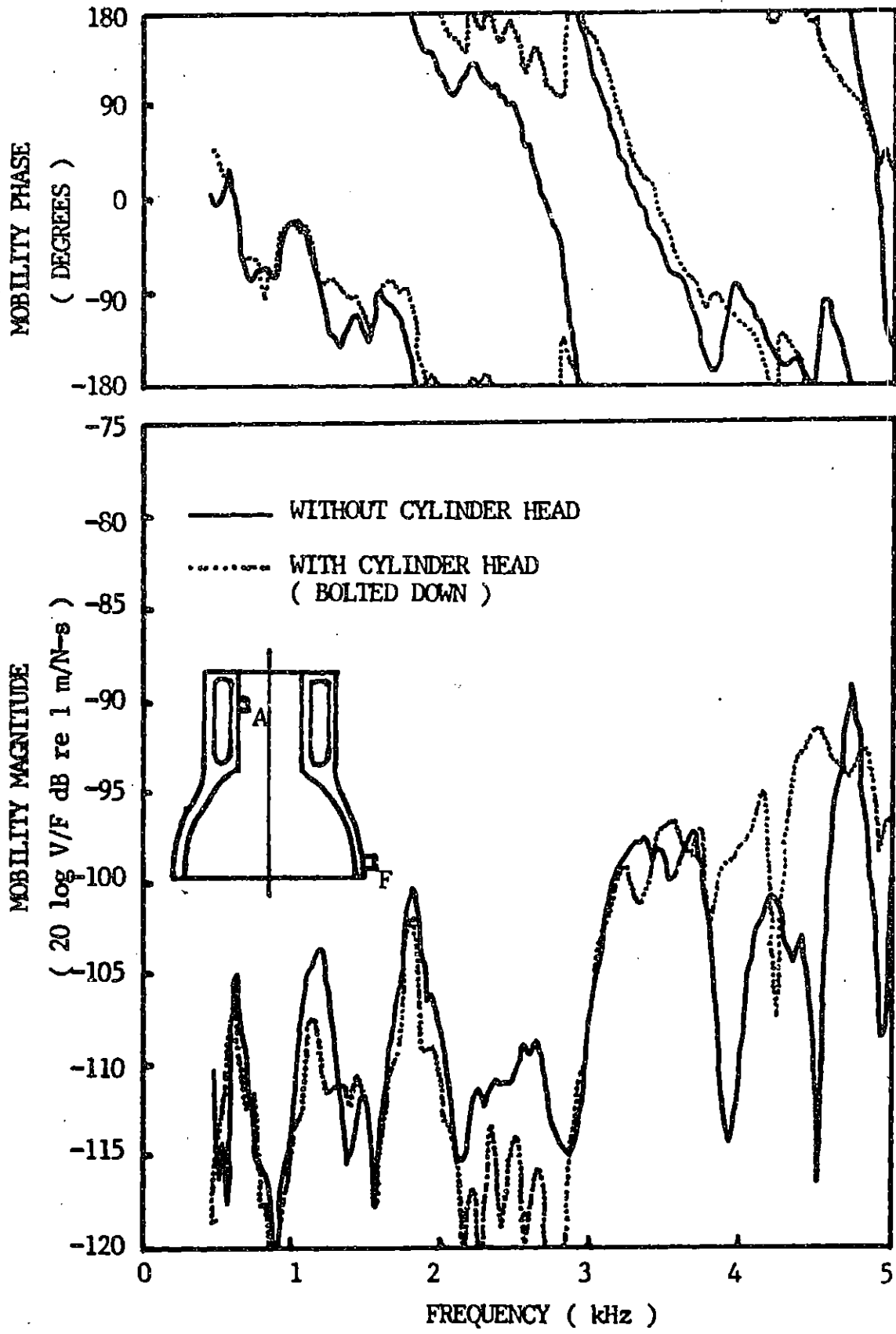
FIGURE 4.8 : EFFECT OF THE PRESENCE OF THE CYLINDER HEAD
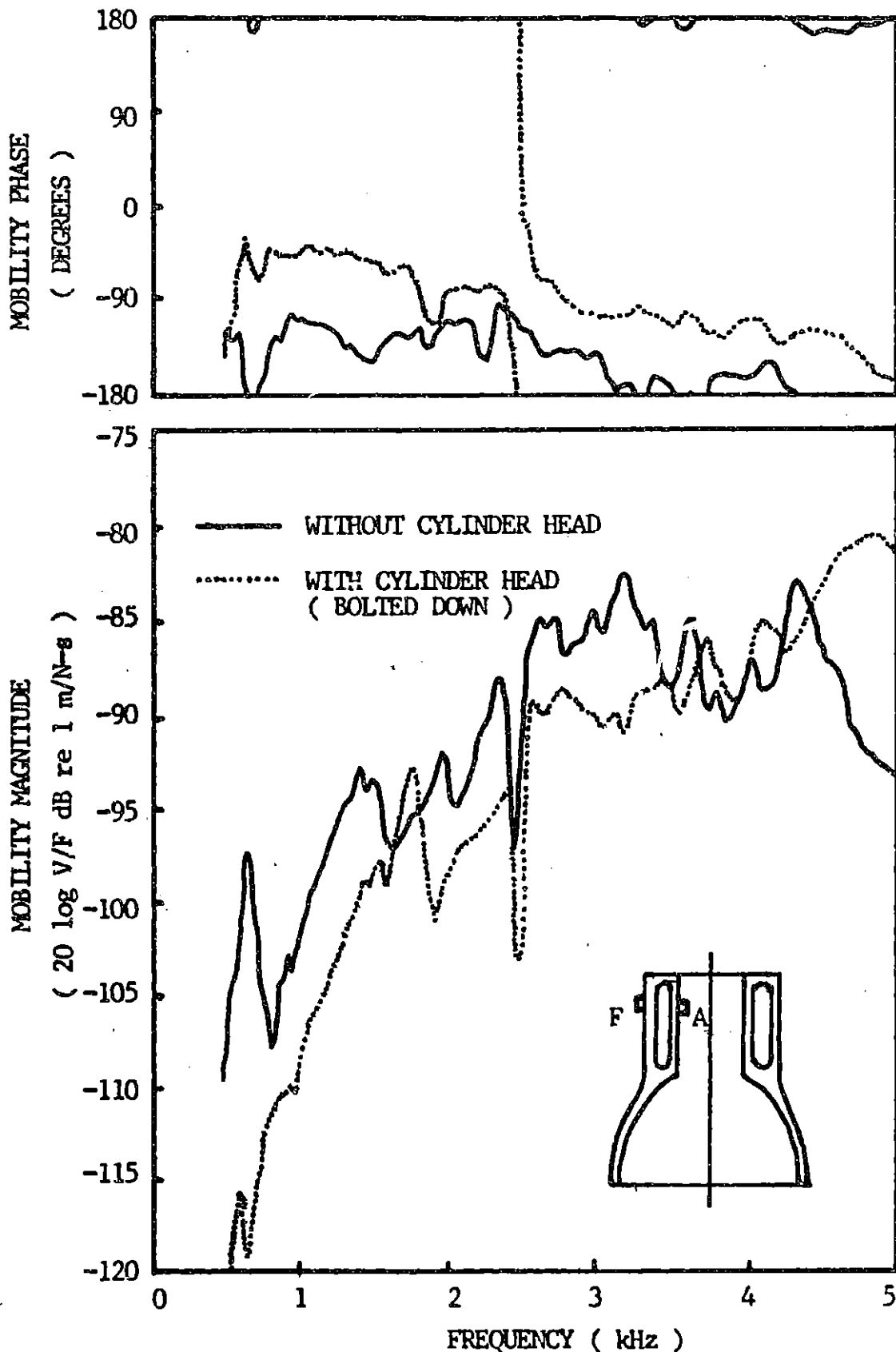ON THE TRANSFER MOBILITY (B2LL – 2R50)

FIGURE 4.9 : EFFECT OF THE PRESENCE OF THE CYLINDER HEAD
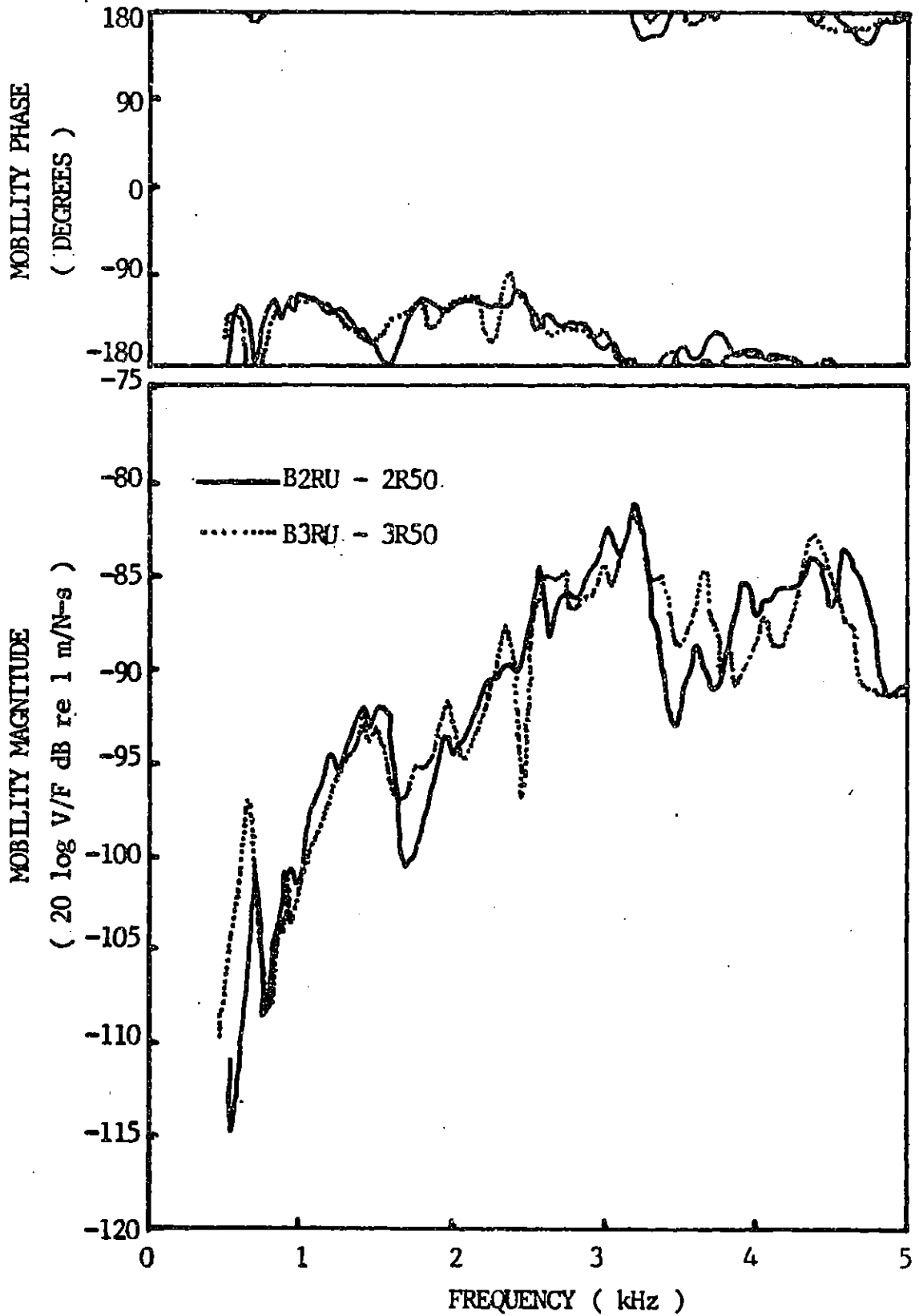ON THE TRANSFER MOBILITY (B3RU – 3R50)

FIGURE 4.10 : TRANSFER MOBILITIES FROM BLOCK SURFACE POINTS
TO THE CYLINDER WALL   (DIFFERENT CYLINDER)

For the transmission path which is near to the cylinder head, the presence of the cylinder head added mass to the transfer mobility in the lower frequency range and damping in the higher frequency range. For the transmission path to the lower block surface, a much less significant effect was observed, particularly in the lower frequency range. This suggests that in the lower frequency range there are two fairly independent transmission paths for the vibrational energy, and that the cylinder head does not significantly affect the lower path.

But in both cases, if the cylinder head was bolted on the cylinder block, the high frequency transmission was increased. Apparently attaching the cylinder head increases the rigidity of the upper deck of the cylinder block so that can transmit higher frequencies more easily.

The role of the cylinder head is summarized as follows:

(1) it has a significant mass effect on the transfer path to the upper portion of the cylinder block surface

(2) it has a significant damping effect in the frequency range above 2 kHz.

(3) it can make system able to carry more high frequency components by adding the rigidity on the upper deck of the cylinder block.
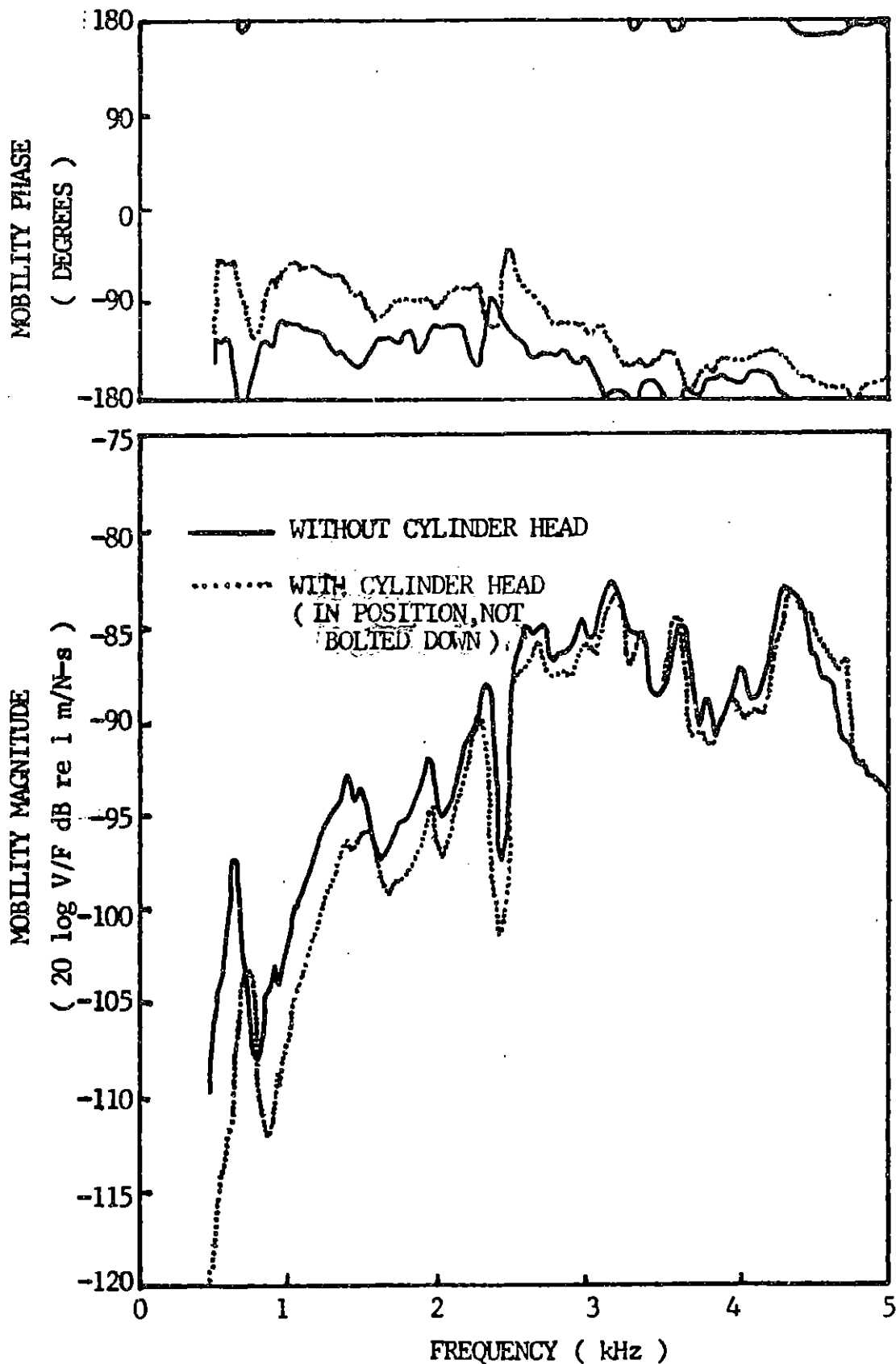
FIGURE 4.11 : EFFECT OF PLACING THE CYLINDER HEAD ON THE
TRANSFER MOBILITY (B3RU – 3R50)

The effects of (1) through (3) were separately observed by comparing Fig. (4.9) and Fig. (4.11). Figure (4.11) was obtained by placing the cylinder head on the cylinder block. It shows only mass effect on that transfer path. The effects of (2) and (3) were obtained by tightening the cylinder head bolts (Fig. (4.9)).

This implies that in the higher frequency range the upper deck of the cylinder block plays a very important role in the transmission path from inside the cylinder to the outer surface of the cylinder block, even if the surface point in question is far away from the cylinder head.

4.3.5 Transmission paths of piston slap noise to the engine surfaces

Fig. (4.12) shows the transfer mobilities for two cylinder block surface points and one cylinder head surface point to the cylinder liner wall. Experiments were done on the right side of the engine and the block surface points lined up with the corresponding cylinder center line. Both cylinder block measurements were done with the cylinder head removed.

It is clear that the major transmission path of piston slap noise is to the upper portion of the cylinder block, even if the effect of the cylinder head is subtracted off. It can be said that the energy transmitted from the cylinder liner wall to the cylinder head surface is negligible. The small contribution of the cylinder

- 69 -

head to the transmission of piston slap noise was reported by W. F. Griffiths et al. [20] for the running engine.

Since the basic structure of the cylinder head is a box stiffened by a combination of lateral and horizontal beams, the cylinder head is considered to be about as rigid as the upper deck of the cylinder block (See Section 4.3.4). If those two elements were directly coupled, the similar magnitudes of the transfer mobilities should be obtained for the two transfer paths; i.e., the one from the upper portion of the block wall to the cylinder wall and the one from the cylinder head surface to the cylinder wall. The coupling of those two elements, however, is not direct, but is provided by the head bolts and the head gasket.

Effect of the cylinder head bolts was observed in Fig. (4.9) on the transmission path through the upper deck of the cylinder block. However, completely different effect was obtained on the transmission path through the cylinder head (Fig. 4.12). Therefore, the cylinder head appears to be resiliently mounted to the block. Further test would be necessary for conclusive proof, but it is possible that the head bolts and gasket constitute a resilient mounting. At any rate, the transmission path of piston slap noise to the cylinder head is insignificant.
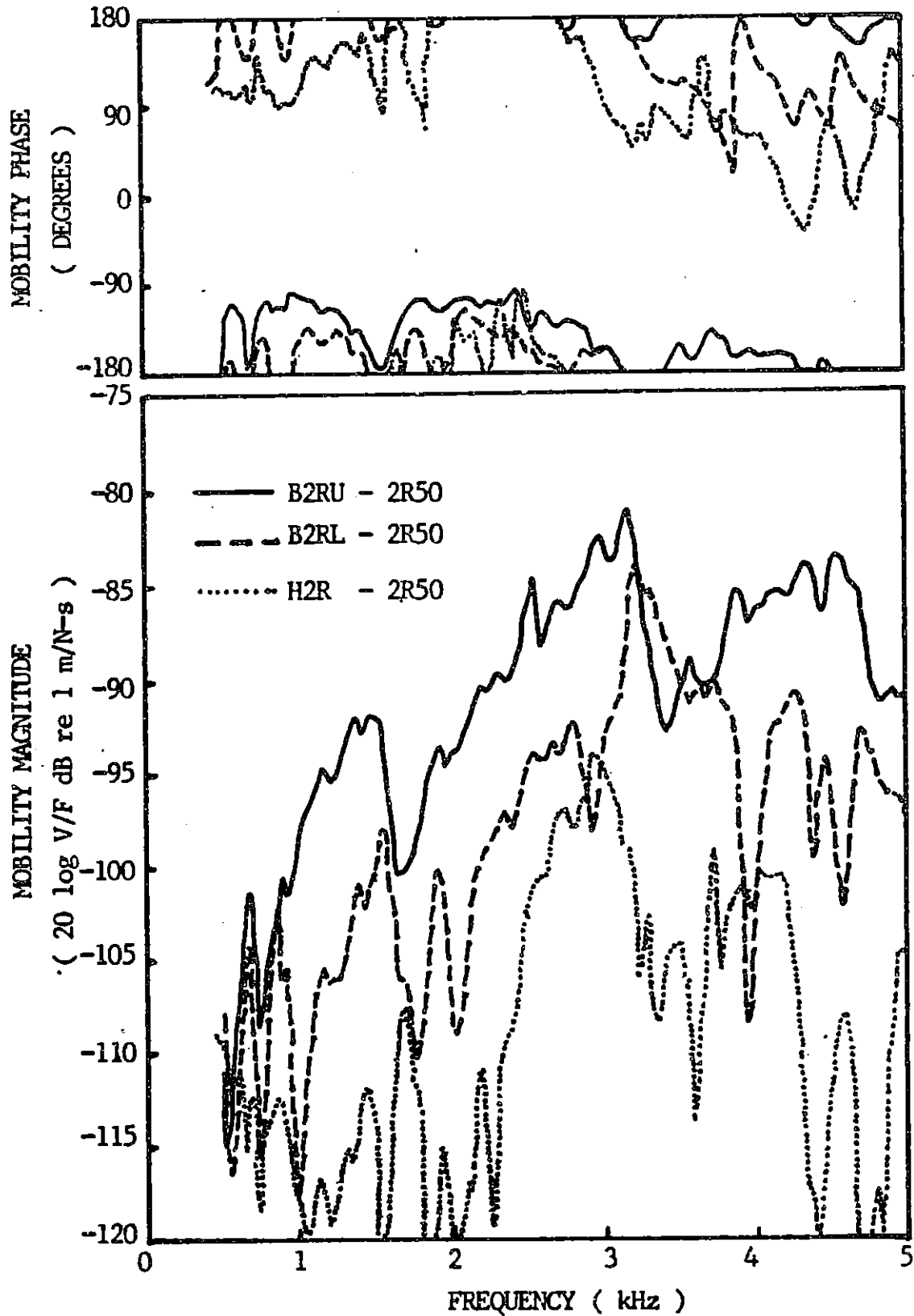
FIGURE 4.12 : TRANSFER MOBILITIES FROM ENGINE SURFACE POINTS
TO THE NO.2 CYLINDER WALL

This result suggests that for reducing piston slap noise, attention should be focussed on the cylinder block. The cylinder head could remain the same and the covers mounted on the cylinder head could remain the same as long as they don't have resonances around 3 kHz.

4.3.6 Transmission paths of piston slap noise through the cylinder block

As discussed in the previous section, the cylinder block plays the major role in transmission of piston slap noise. In this section, various test results are shown and compared in order to obtain the major transmission path of the piston impact force. Since for ease of access these tests were carried out without attaching the cylinder head, the effect of such attachment should be taken into account for the transfer mobility magnitudes obtained at the upper portions of cylinder block.

Fig. (4.13) to Fig. (4.16) show transfer mobilities from No. 1 and No. 2 cylinder to various surface points. The accelerometer positions correspond to the locations of the major slaps. Transfer mobilities to the right and left surfaces are shown on separate figures.

Since the No. 1 and No. 2 cylinders are different in their

construction, (the No. 1 cylinder is next to the rigid front wall of the block), the transfer mobilities differ for corresponding paths. Still, both figures show that the transmission path to the upper portion of the cylinder block is predominant. Fig. (4.16) shows the magnitude of the transfer mobility from B2LL (oil pan joint) to 2R50 is very small.

From these figures, the following conclusions are drawn:

(1) The major transfer path of the piston slap noise is to the upper portion of the cylinder block surface nearest to the cylinder in which piston slap occurs.

(2) The transfer mobilities to the other block surfaces are considerably lower than that of the major path.

(3) The transfer mobility to the oil pan joint is negligible so that the oil pan could not be excited by the piston slap impacting force if it has sufficiently low response in the frequency range of interest (1 to 4.5 kHz).

These results indicate that the cylinder wall can be modeled as a beam supported at the lower deck of the cylinder block. As discussed in Section 4.3.4 the upper deck of the cylinder block is rigid enough and it carries most energy of the piston impact so
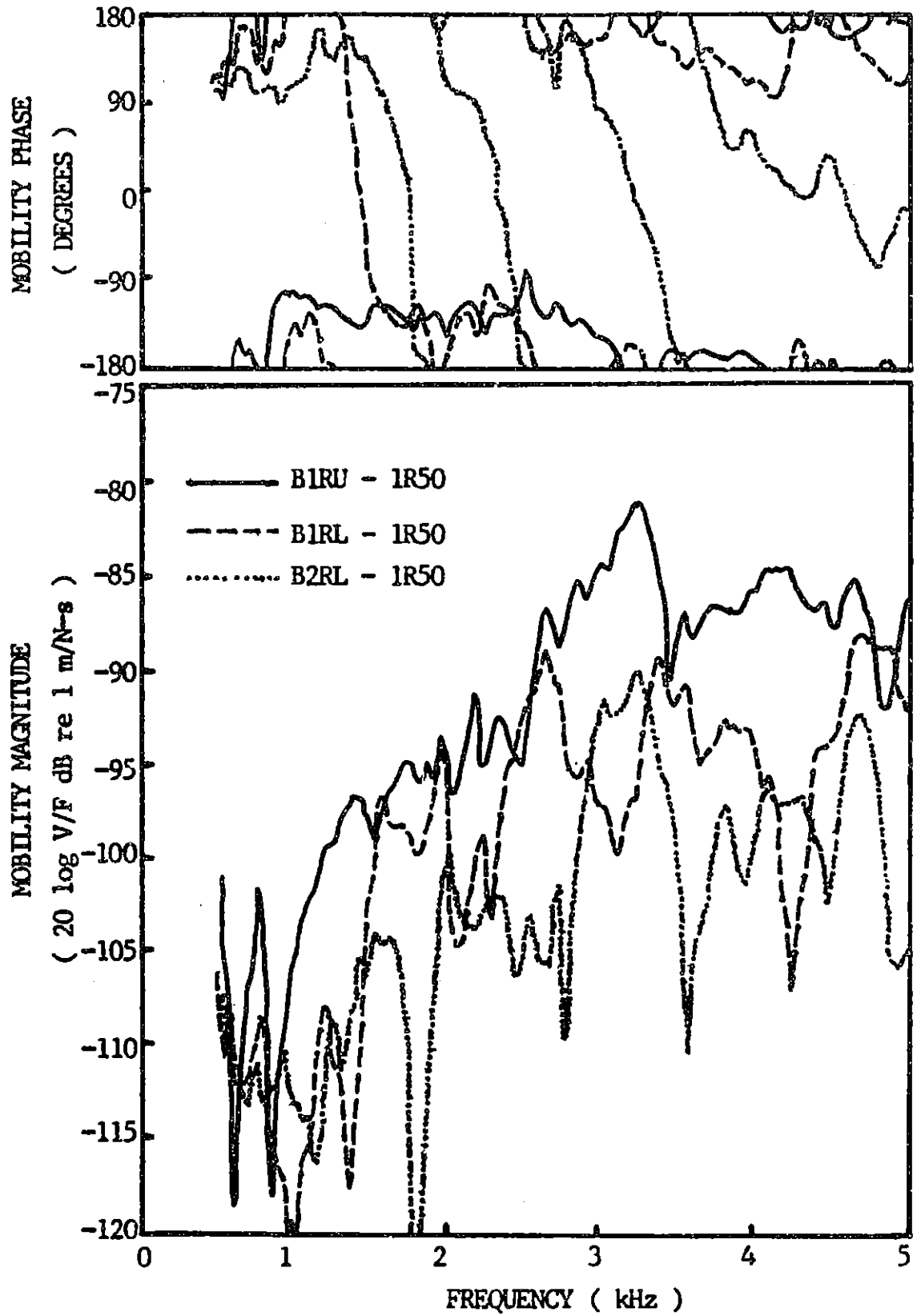
- 73 -

FIGURE 4.13 : TRANSFER MOBILITIES FROM RIGHT SURFACE POINTS
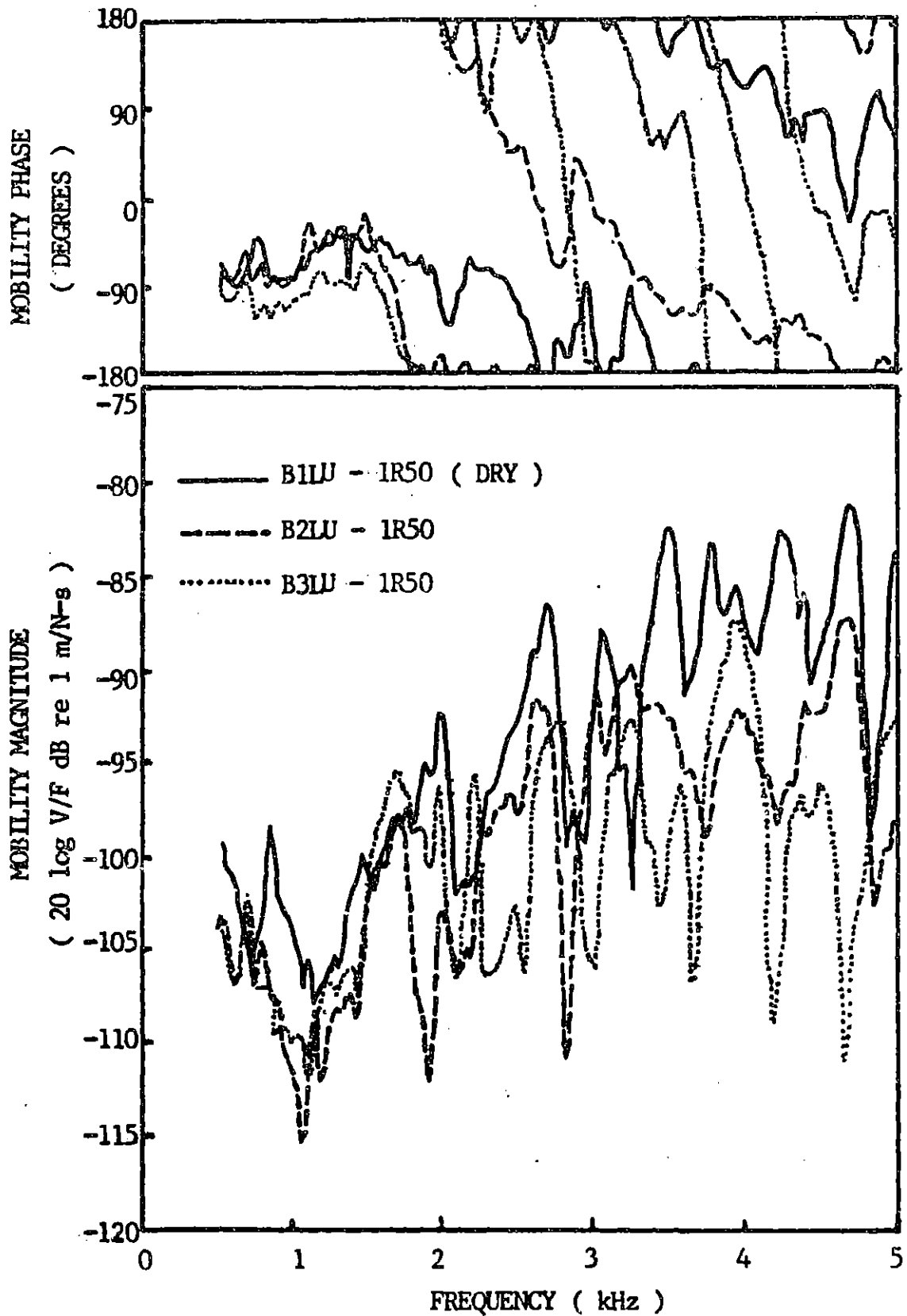TO THE NO.1 CYLINDER WALL

FIGURE 4.14 : TRANSFER MOBILITIES FROM LEFT SURFACE POINTS
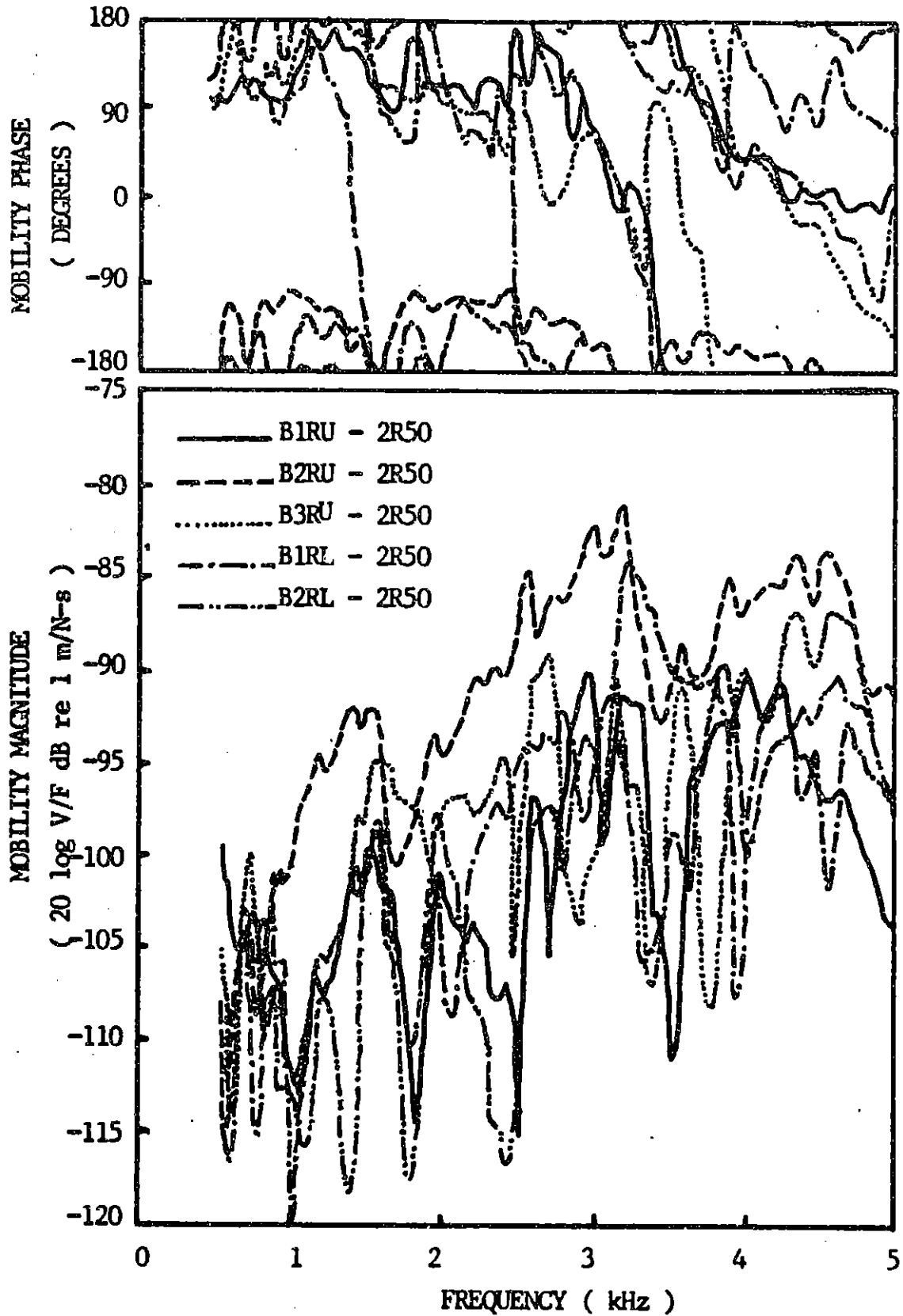TO THE NO.1 CYLINDER WALL

- 75 -

FIGURE 4.15 : TRANSFER MOBILITIES FROM RIGHT SURFACE POINTS
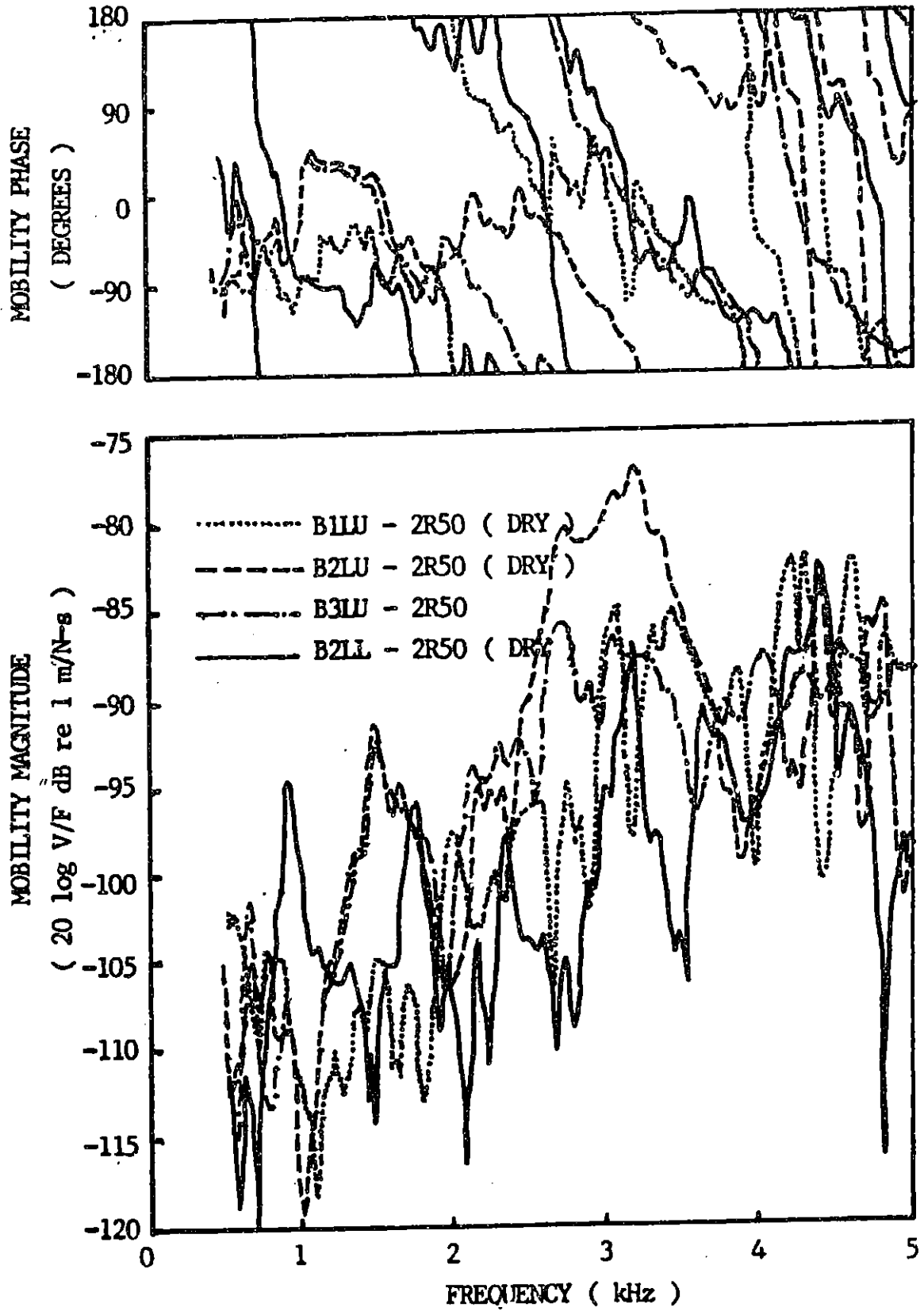TO THE NO.2 CYLINDER WALL

FIGURE 4.16 : TRANSFER MOBILITIES FROM LEFT SURFACE POINTS
TO THE NO.2 CYLINDER WALL

that the beam is excited at the upper deck of the cylinder block.
Experiments estimating the stiffness of the cylinder block show
that the stiffness of the cylinder block is low between upper and
lower deck [27]. This suggests that stiffening the cylinder
block wall would help to reduce the emitted noise due to piston
slap.

4.3.7 Effect of the presence of the cylinder liner sleeve

As shown in Table (4.1), the Isuzu engine employs a dry
liner and the John Deere engine employs a wet liner. The dry liner
engine has a thin wall cylindrical sleeve press-fit into the liner
bore in the cylinder block casting. In this case, all the surface
of the liner sleeve is kept in contact with the liner bore so as
to maximize metal to metal heat transfer. The wet liner type engine
has a much thicker liner supported by the cylinder block at the
upper deck only.

The major differences between two versions are:

(1) The dry liner is supported by upper and lower deck
    of the cylinder-block like a double-cantilever, but
    the wet liner is considered to be cantilevered at
    the upper deck only and unsupported by the soft
    material used for sealing the liner to the lower deck.

- 78 -

(2) The wet liner is exposed to the cooling water, but the dry liner is separated from the cooling water by the cylinder wall.

To illustrate the effect of the presence of the cylinder liner sleeve, two measurements were done and compared on the Isuzu engine. The liner sleeve was removed and the transfer mobility was measured in the same manner as testing the engine. The liner sleeve was placed onto a foam pad, and the impedance head was epoxied to the outer surface of the sleeve 10 mm from the top. The accelero-meter was attached inside the liner sleeve 50 mm from the top; the same measurement point as when the liner was installed in the cylinder block.

The literature (28) suggests that below its ring frequency a cylinder can be treated as a beam. The ring frequency is given by the equation,

$$f_r = c_L/2\pi R$$

where

f_r: ring frequency (Hz)

c_L: longitudinal wave speed (m/s)

R: radius of the cylinder (m) ,

For the liner sleeve of the Isuzu engine, the ring frequency is cal-culated as f_r = 19 kHz, which is much higher than the upper
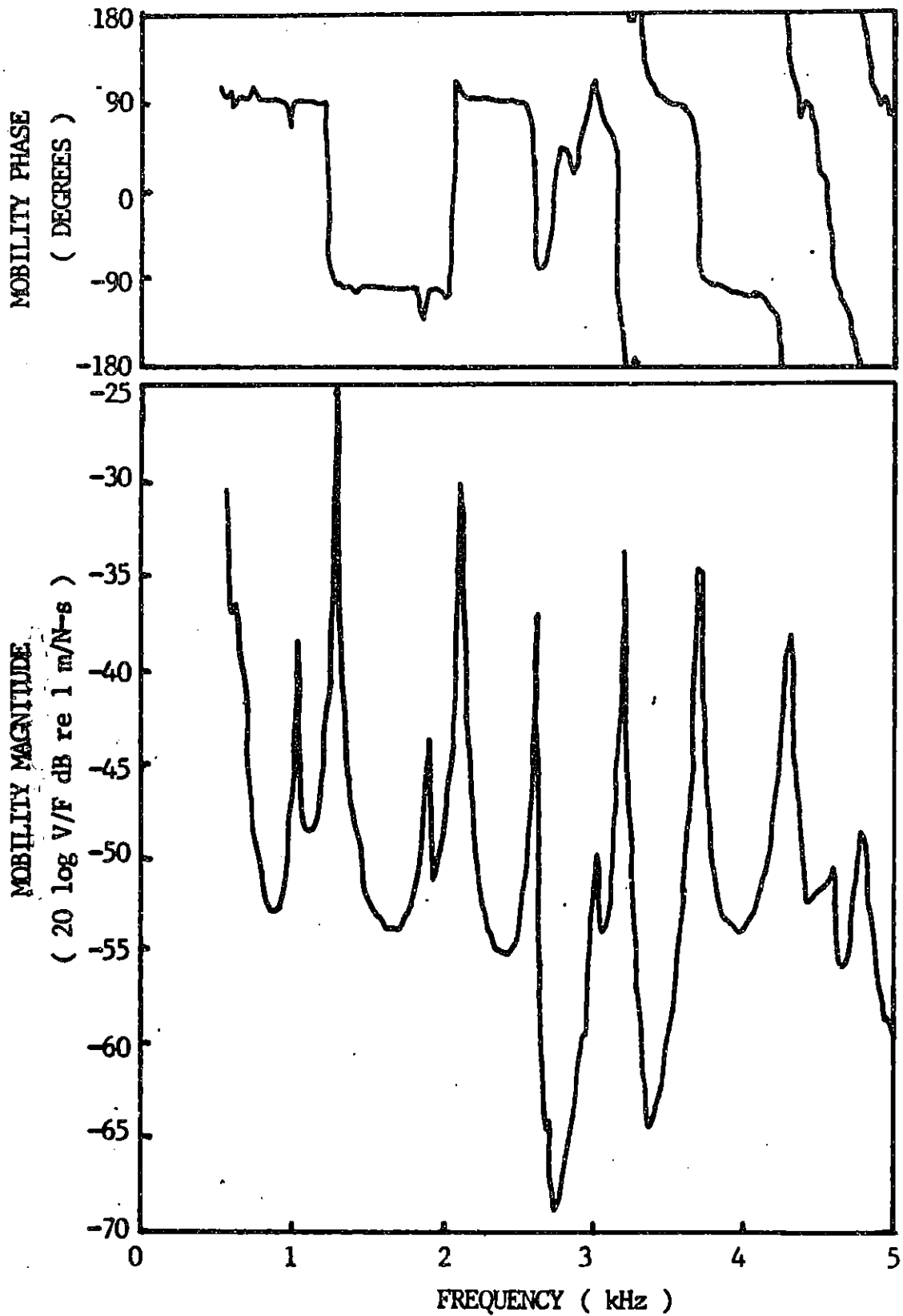
FIGURE 4.17 : TRANSFER MOBILITY OF THE CYLINDER LINER SLEEVE

frequency range of interest. As was expected, the liner sleeve can be considered as a beam. (See Fig.(4.17).)

For the cylinder block, the accelerometer was attached inside the liner bore 50 mm from the top surface, (the distance between the impedance head and the accelerometer was shortened by sleeve wall thickness of 1 mm a negligible distance for the purpose of these experiments). Fig. (4.21) shows that the difference in the distance does not affect the transfer mobility in this portion of the liner wall.

The transfer mobility obtained after removing the liner sleeve is compared in Fig.(4.18) with corresponding transfer mobility with the liner sleeve in place. A signi..cant difference was obtained between the two spectra in the frequency range of 2 - 3 kHz. The mobility phases were similar to each other in the entire frequency range. The difference between the two measurements was the presence of the cylinder liner sleeve and the stress field around the liner sleeve introduced by press-fitting. The difference in position of the accelerometer could be neglected as mentioned above. The difference in static stress field cannot affect the dynamic properties of the structure.

Therefore, the difference obtained is considered to be due to the characteristics of the attaching surface of two elements. The possible mechanism is the interface damping at the attaching
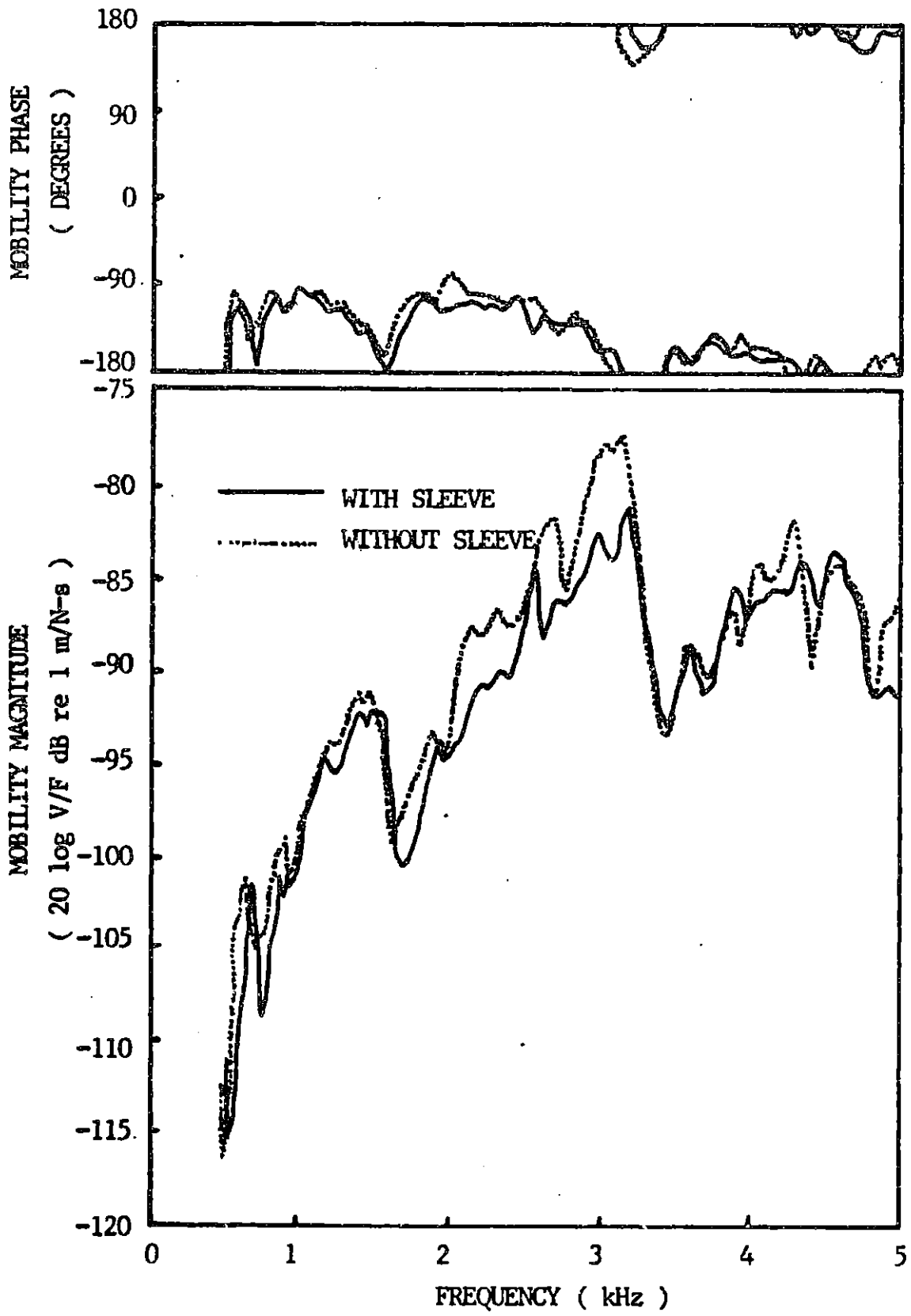
FIGURE 4.18 : EFFECT OF REMOVING THE LINER SLEEVE ON THE
TRANSFER MOBILITY (B2RU - 2R50)

surface; however, further experiments, such as the input impedance
of both the liner sleeve and the cylinder bore surfaces, are
needed to confirm this assumption.

One can notice by comparing Fig.(4.17) and Fig.(4.18) that
most of the peaks in the magnitude of the transfer mobility from
the cylinder block surface to the cylinder liner wall coincides with
the resonances of the liner sleeve. The rest of the peaks are
considered to be due to the cylinder block outer surface which can
be treated as a beam.

Those considerations lead to the model of the cylinder
block discussed in Section 5.2.3:

    (1)   the cylinder liner is treated as a beam

    (2)   the upper deck of the cylinder block is treated as
         a rigid body

    (3)   the cylinder block surface is treated as a beam.

The following comparison was made between two engines.
Although the results are not directly comparable due to differences
in basic design, the differences between two similar paths measured
on each engine can be compared.

Fig. (4.19) and Fig. (4.20) show the transfer mobilities
from engine surface to the right upper and left lower surface of the

cylinder liner walls of the Isuzu and John Deere engines, respectively. Because the major transfer path of the piston slap noise is cylinder liner wall to the engine surface through the upper deck of the cylinder block, the difference in mobility is mainly due to the construction of the cylinder liner itself. For the Isuzu engine, the significant difference in mobility magnitude is observed above 2 kHz. For the John Deere engine, the greatest difference can be seen in the 2.5 to 4 kHz range with less difference both above and below that range.

The other notable difference between the two engines is the magnitude itself, even if allowing for the effect of the cooling water. (The John Deere engine was tested without water and the Isuzu engine was tested with water.) As shown in Table 4.1 the John Deere engine has a much heavier cylinder block than the Isuzu engine. If one creates a lumped paramter model for each transfer path, the mass for the John Deere engine should be larger than that for the Isuzu engine. If the other elements in the lumped model are the same, the transfer mobility of the John Deere engine should be smaller than that of the Isuzu engine due to the mass-effect. Additionally, those figures show the difference in the damping added to each transfer path. The transfer mobility of the Isuzu engine (Fig. (4.19)) represents much more damped system.

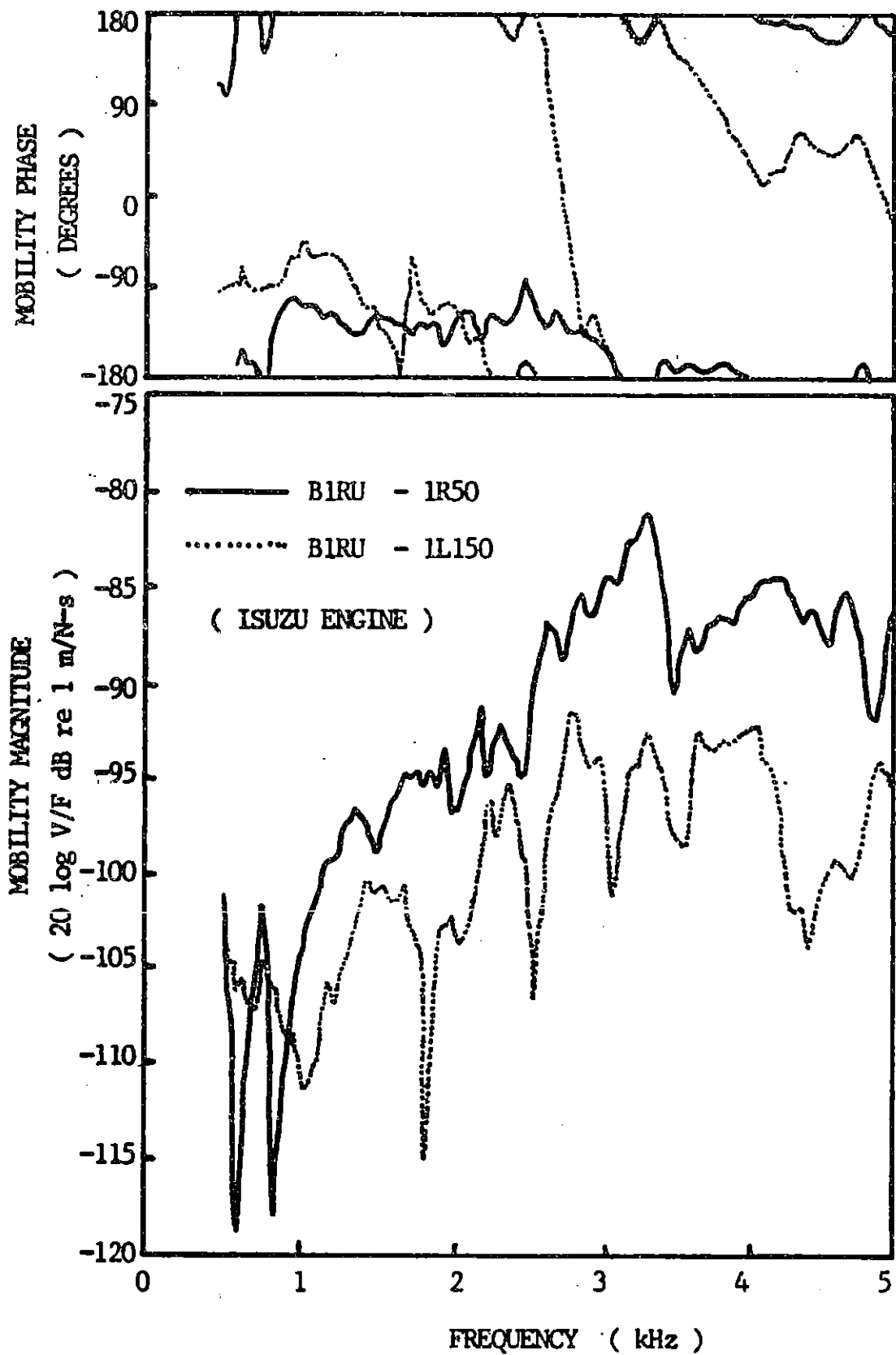The differences discussed above are considered to be due to

FIGURE 4.19 : TRANSFER MOBILITIES FROM THE BLOCK SURFACE TO THE UPPER AND LOWER SURFACES OF THE CYLINDER WALL
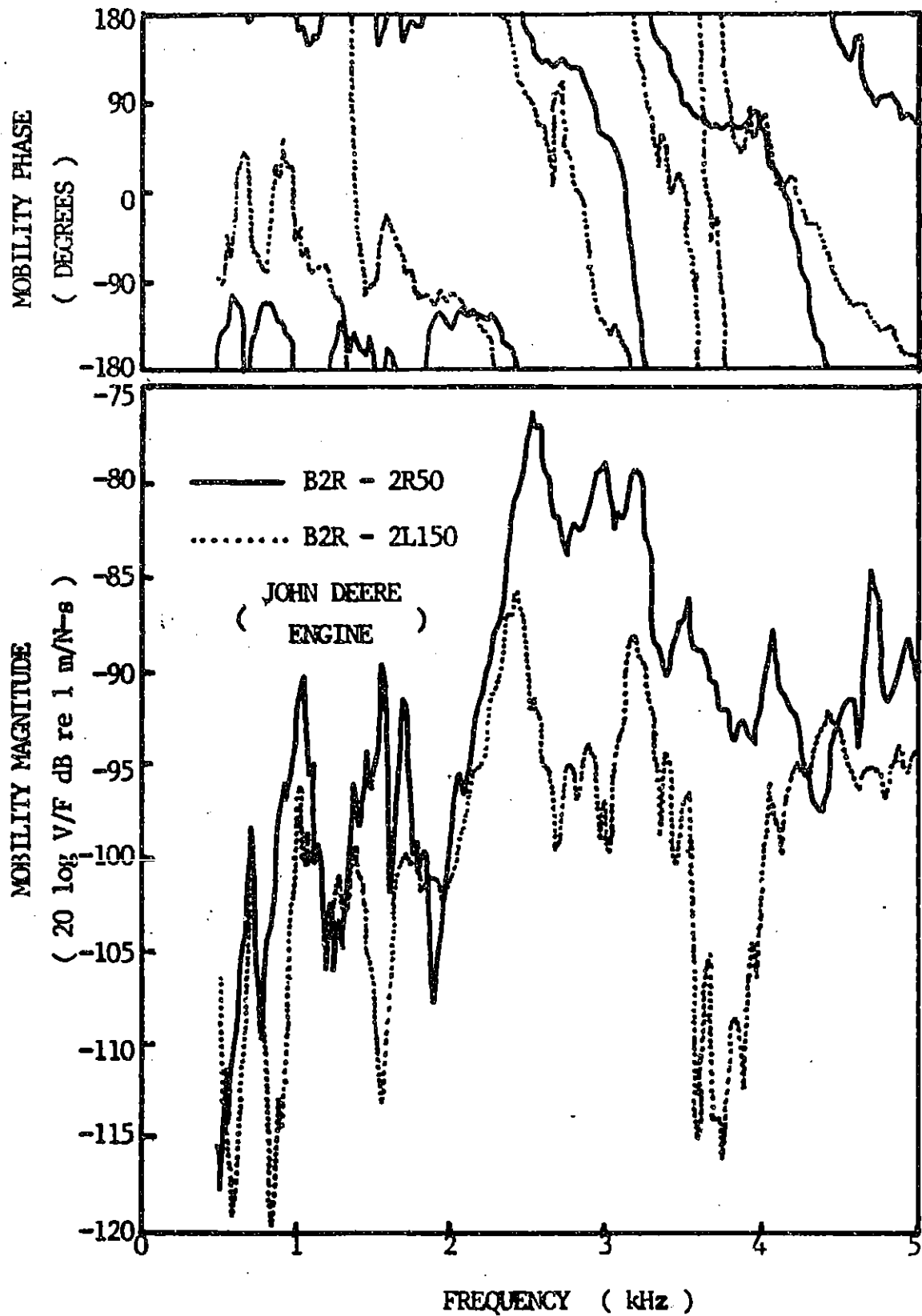
FIGURE 4.20 : TRANSFER MOBILITIES FROM THE BLOCK SURFACE TO THE
UPPER AND LOWER SURFACES OF THE CYLINDER WALL

the difference in construction of the dry-type versus wet-type liner. The wet-type liner is readily treated as a beam clamped at one end and free at the other, unlike the dry-type liner which can be treated as a beam clamped at both ends.

4.3.8 Effect of the location of the accelerometer on the transfer mobility

As mentioned in Section 1.3.2 the most widely accepted technique for reducing the piston slap noise is piston pin offset. Offsetting the piston pin changes the nature of the piston slap insofar as it changes the timing of the piston slap initiation which results in a change of the impacting energy. The following experiments were carried out to determine which factor, slap location or slap energy, has the most effect on emitted piston slap noise.

The experiments were done on both the Isuzu and the John Deere engine. The impedance head was kept fixed on the cylinder block surface point, and successive measurements were done by changing the distance of the location of the accelerometer from the top surface of the cylinder block. The results are shown in Fig. (4.21) through Fig. (4.23). Each figure shows similar mobility magnitude and phase. Especially, Fig. (4.21) and Fig. (4.22) show basically the same transfer mobilities to the

different liner surfaces.

The distance of 50 mm was assumed to be the most likely location of the piston slap since that is the piston pin location at top dead center from both engines. The other positions of the accelerometer were chosen as 10 mm and 20 mm below the prescribed point. These points correspond to the piston pin locations at crank angles as shown in Table 4.2.

Figures (4.21) through (4.23) suggest that the reduction of piston slap noise by employing piston pin offset comes from reducing the impacting energy, and not from changing the impacting location, since the transfer mobility does not change within a wide range of crank angle. This result supports the conclusion that emitted piston slap noise correlates to the impacting energy only as reported by T. Usami et al. [24].
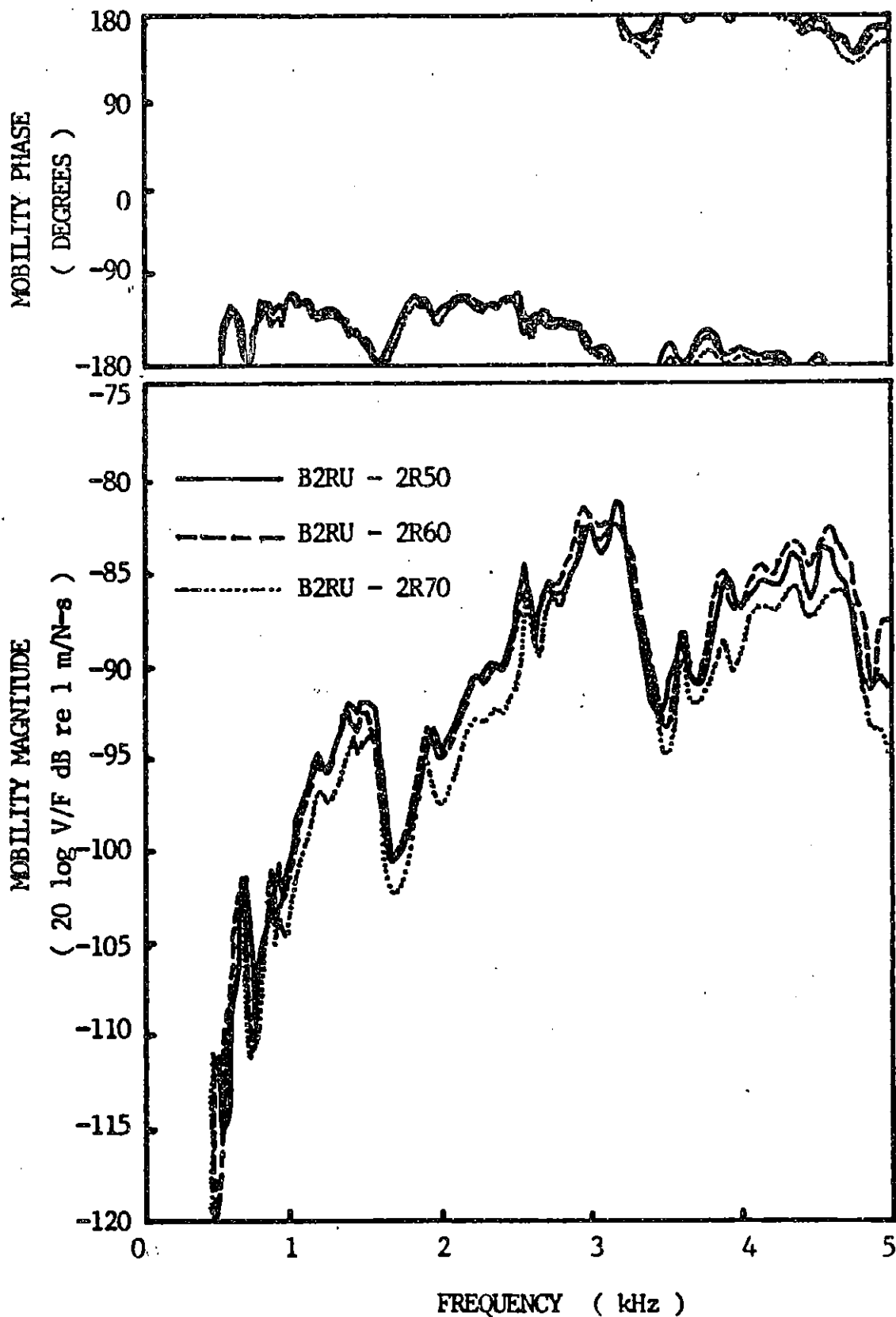
FIGURE 4.21 : EFFECT OF THE ACCELEROMETER LOCATION
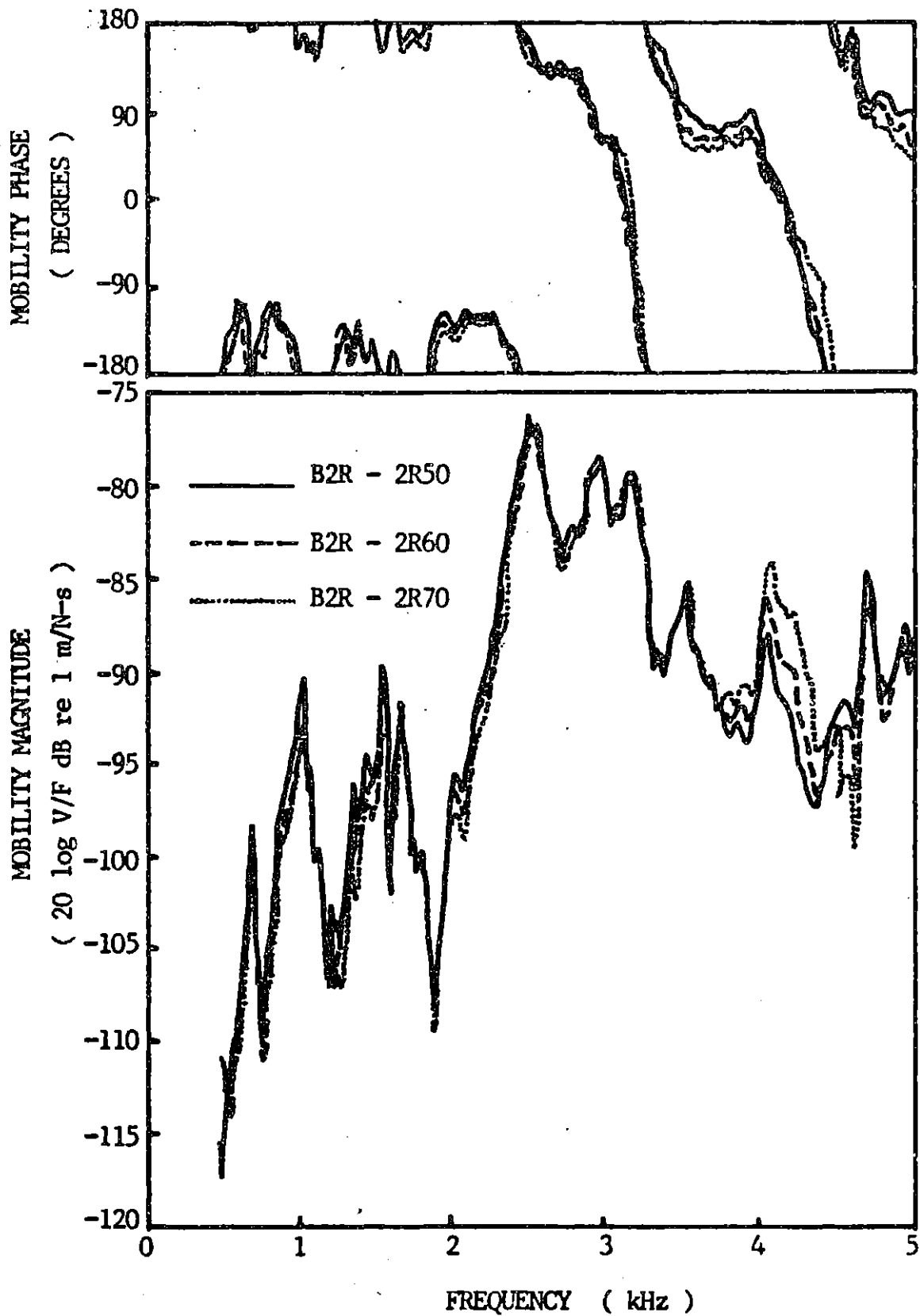ON THE TRANSFER MOBILITY (ISUZU ENGINE)

FIGURE 4.22 : EFFECT OF THE ACCELEROMETER LOCATION
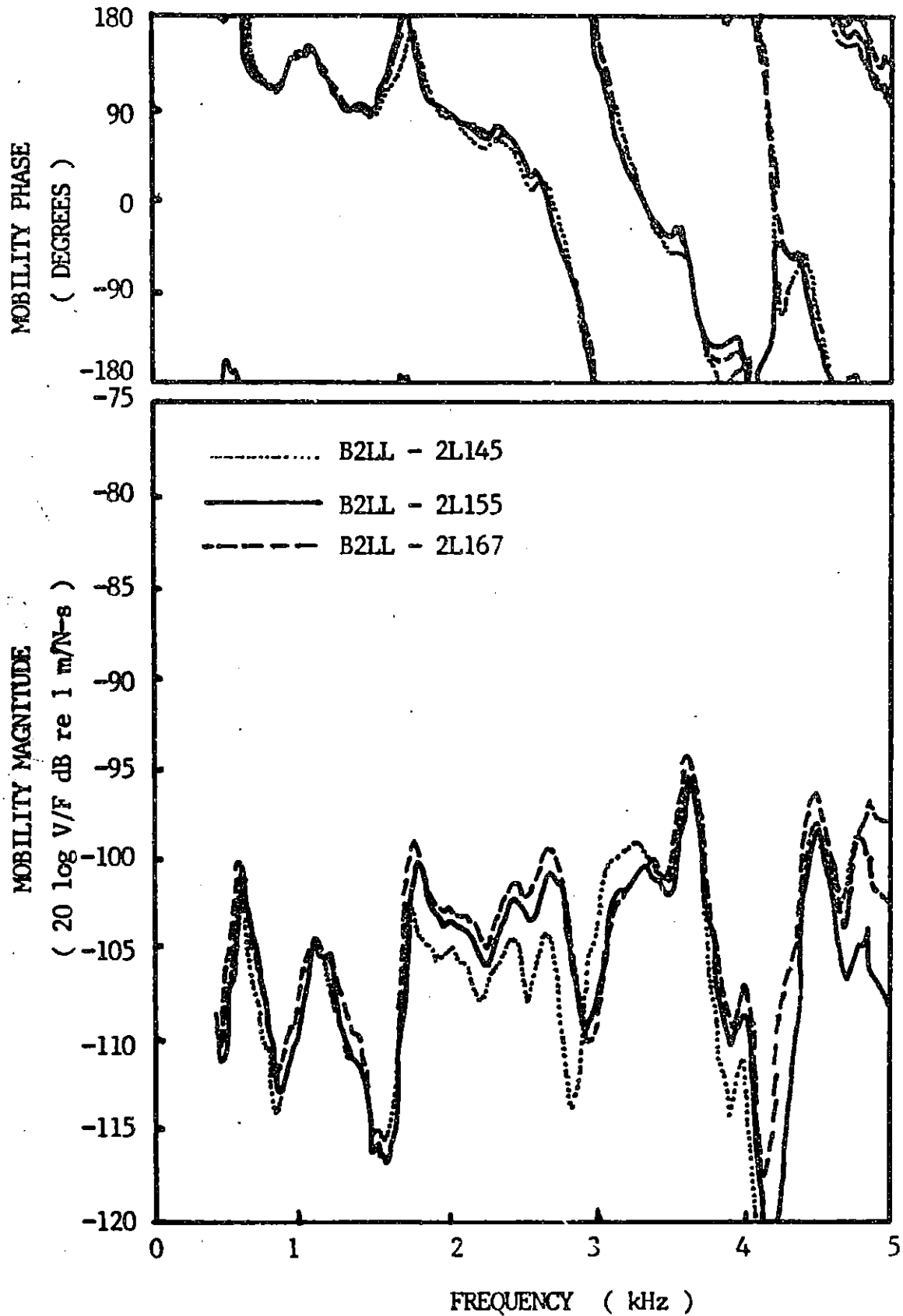ON THE TRANSFER MOBILITY (JOHN DEERE ENGINE)

FIGURE 4.23 : EFFECT OF THE ACCELEROMETER LOCATION
ON THE TRANSFER MOBILITY (ISUZU ENGINE)

PISTON PIN LOCATION FROM THE TOP SURFACE OF THE CYLINDER BLOCK (mm)	CORRESPONDING CRANK ANGLES (DEGREES CRANK ANGLE)	
	ISUZU	JOHN DEERE
50	T.D.C.	T.D.C.
60	32 A.T.D.C.	31 A.T.D.C.
70	46 A.T.D.C.	45 A.T.D.C.

T.D.C. : TOP DEAD CENTER

A.T.D.C. : AFTER TOP DEAD CENTER

TABLE 4.2 : RELATIONSHIP BETWEEN THE PISTON PIN LOCATION AND THE CRANK ANGLE

CHAPTER 5

CONCLUSION AND SUGGESTIONS FOR FURTHER WORK

In this chapter, the experimental results are summarized and possible ways of reducing piston slap noise are discussed.

5.1 Summary of the Experiments

The experiments were designed to determine the major transmission path of the piston slap noise in the frequency range of 1 to 4 kHz where the piston slap noise is considered to be the predominant noise source in the engine.

5.1.1 The major transmission path of the piston slap noise

As discussed in Section 4.3.6, the transfer path of the major piston slap impact, which occurs around the top dead center, is as follows:

(1) the piston impacts the cylinder liner wall

(2) the cylinder liner transmits this energy to the upper deck of the cylinder block

(3) the upper deck of the cylinder block transmits this energy and excites the cylinder block wall (most energy is emitted from the upper portion of the block wall due to its construction).

Since these conclusions result from the experiments on the dry-liner type engine, this transfer path should be general to existing conventional water cooled engines. Although it is possible that for the dry-liner type engine some of the impacting energy is transmitted through the lower deck of the cylinder block, this is impossible for the wet-liner type engine due to the use of resilient materials for lower end support and sealing rings. The lower deck path contributes much less than the major transfer path discussed above in terms of carrying the impacting energy. Piston slap noise is primarily radiated in the region near the impacting cylinder. The transmission of the piston slap noise to the cylinder head and the oil pan are negligible.

5.1.2 The factors which affect the transfer mobility of the major transmission path

The presence of the cylinder head has a significant effect on the transfer mobility, but this is not due to the cylinder head itself. The factor which affected the transfer mobility was the additional damping in the transfer path introduced by tightening the cylinder head bolts. A similar effect, but less significant, was observed by measuring the transfer mobility from the lower surface of the cylinder block to the lower portion of the cylinder liner wall. In this case, the main cap bolts played the same role as the head bolts.

The presence of the liner sleeve affected the transfer mobility. This may result from the interface damping at the interface of the liner sleeve and the cylinder bore surface. However, further work is needed to clarify the vibration attenuation mechanism at the interface.

5.2 Further Work

Based on the analysis of the transmission path discussed in the previous chapters, the following further work is recommended toward the reduction of piston slap noise.

5.2.1 Reduction of piston slap no..e at the source

As discussed in Section 4.3.8 piston slap noise will not be reduced greatly by changing the piston slap location. Work aimed at treating the source should be concentrated on reducing the energy released when the piston hits the cylinder liner wall. The following factors should be taken into account for these studies:

(1) Dynamic clearance between the piston and the cylinder liner.

(2) Indicator diagram, or pressure force versus crank angle.

(3) Input impedance of the cylinder liner wall.

5.2.2 Reduction of piston slap noise by treating its transmission
       path

Since the major transmission path of piston slap noise
consists of only one element for the dry-liner type engine (the
block casting) and two for the wet-liner type engine (the block
and the liner), reducing the piston slap noise by treating its
transmission path is rather more difficult than treating the
transmission path of the combustion noise for which the resilient
main bearing was discussed in ref. 25.

The same technique may be applied to the wet-liner type
engine by employing a resilient material at the upper deck of the
cylinder block. But in this case, the greatest care must be taken
with the design, because the failure of this part would constitute
total failure of the engine.

Another technique which the experiments suggest is to treat
the interface between the elements such as the cylinder block and
the cylinder liner (or the liner sleeve). However, further experi-
ments are necessary to make a decision on the design changes.

The possible design changes are:

(1) Change the balance of the input impedances of both
     the liner sleeve and the cylinder bore by means of
     changing the thickness of both walls.

(2) Control the area of the interface

Both methods are applicable to both the wet and dry liner engines.

The key to understanding piston slap noise is the cylinder block, the major element in the transmission path. The test results show the possibility of modeling the major transmission path of the piston slap noise (4.3.7). The basic idea is derived in the next section.

5.2.3 The basic concept in modeling the major transmission path

The natural frequencies of a free free beam in bending are obtained as follows [29]:

$$P_1 \ell = 4.730$$

$$P_{2\ell} = 7.853$$

and as a practical approximation at higher frequencies,

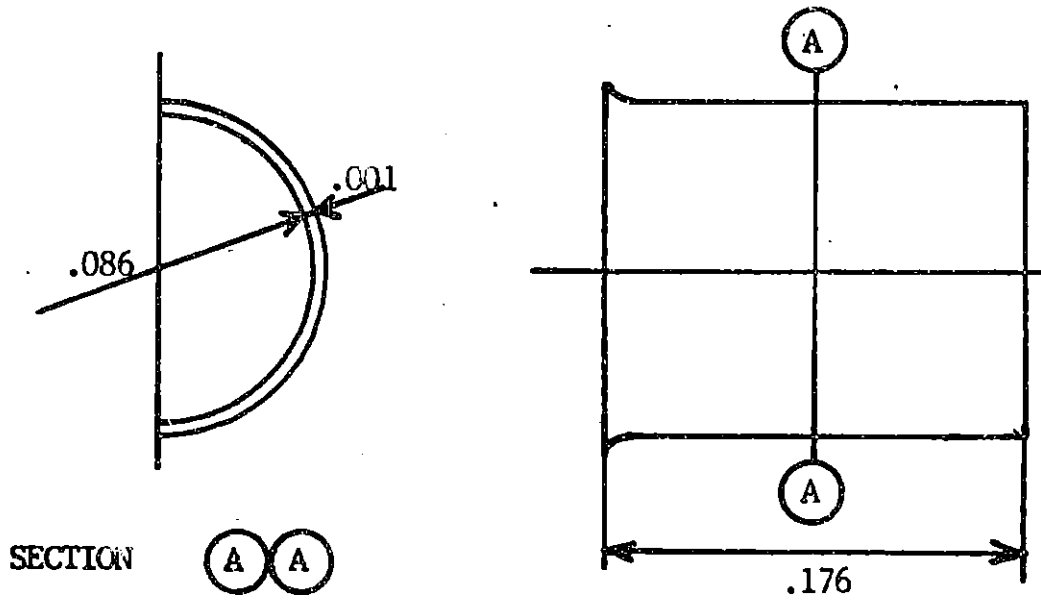$$P_{n\ell} = \pi(n+\tfrac{1}{2}) \text{ for } n \geq 3$$

and the natural frequencies are given by

$$f_n = \frac{1}{2} \sqrt{\frac{EI}{\rho A}} \frac{(P_{n\ell})^2}{\ell^2}$$

where
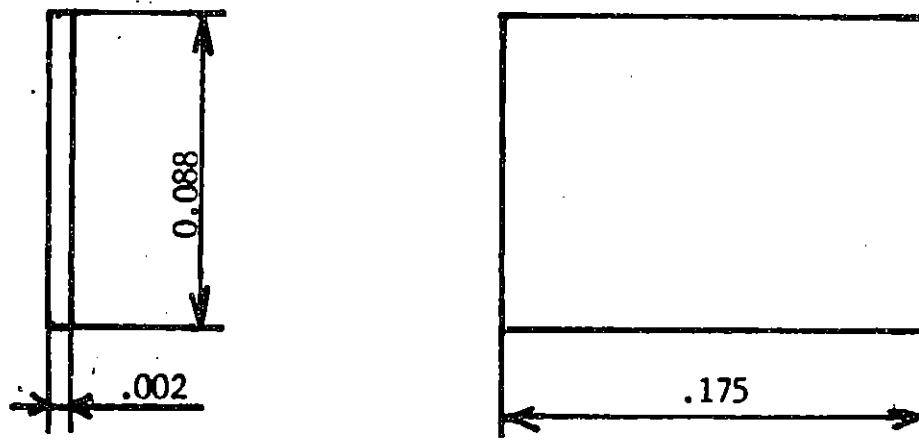
f_n: n^{th} natural frequency in Hz

E: Young's Modulus in N/m^2

SECTION (A)(A)

ACTUAL LINER SLEEVE

BEAM MODEL OF LINER SLEEVE

DIMENSIONS IN m

FIGURE 5.1 : DIMENSIONS OF THE ACTUAL AND MODELED
LINER SLEEVE OF THE ISUZU ENGINE

- 98 -

I: moment of inertia in m^4

ρ: density in kg/m^3

A: cross sectional area in m^2

ℓ: length of the beam in m

P_n: the nth eigenvalue of a free vibration problem

The natural frequencies of the liner sleeve were calculated by modeling the sleeve as a beam with the dimensions shown in Fig. (5.1). The natural frequencies which lie in the frequency band of interest are 1000 Hz and 3240 Hz. Fig. (4.17) shows the corresponding peaks in mobility magnitude at those frequencies.

The cylinder blocks of both engines were modeled in a similar fashion. For the Isuzu engine, the portion of the cylinder block where the liner is fitted and the cylinder block wall were assumed as beams with the dimensions shown in Fig. (5.2(a)), (the wall thickness of the cylinder block at the liner was assumed with the conventional wall thickness obtained by usual casting methods). Both beams were assumed to be clamped at both ends.

Also for the John Deere engine, the cylinder liner and the cylinder block were assumed to be beams with the dimensions shown in Fig. (5.2(b)). In this case the cylinder block wall was considered to be clamped at both ends, but the cylinder liner was considered to be clamped at one end and freely supported at the other end. (For the actual dimensions, see Table 4.1.)

The natural frequencies for these beam models are shown in Table 5.1. It can be seen from this table and the figures of the transfer mobility of the major transfer path (Fig. (4.20) for the Isuzu engine and Fig. (4.21) for the John Deere engine) that, for each engine, the frequency range which shows the largest mobility magnitude coincides with the natural frequencies obtained by beam models.

From the consideration discussed above, the following methods should be effective in reducing the piston slap noise:

(1) Stiffen the cylinder block wall by adding the vertical (parallel to the cylinder center line) ribs, which raises the natural frequency of the wall out of the important frequency range.

(2) Use the resilient material in the transmission path between the cylinder and the block structure.

The beam model discussed above considers only the input and the output part of the transmission path of the piston slap noise. The agreement in the frequency range between the natural frequency of the beam model and the actual frequency range where the transfer mobility magnitude shows the peak suggests this kind of modeling method is helpful in understanding the cylinder block, the major element in the transfer path of the piston slap noise. This model

could be extended by introducing appropriate coupling between the two beams to represent the upper deck of the cylinder block. Such a study might result in finding other factors to be treated for further reducing piston slap noise.

CLAMPED ENDS

.17

.18

FREE END

.111

.102

.127

.118

.006

.016

.006

.016

CYLINDER BLOCK
WALL

CYLINDER LINER

CYLINDER BLOCK
WALL

CYLINDER LINER

(a)
ISUZU ENGINE

(b)
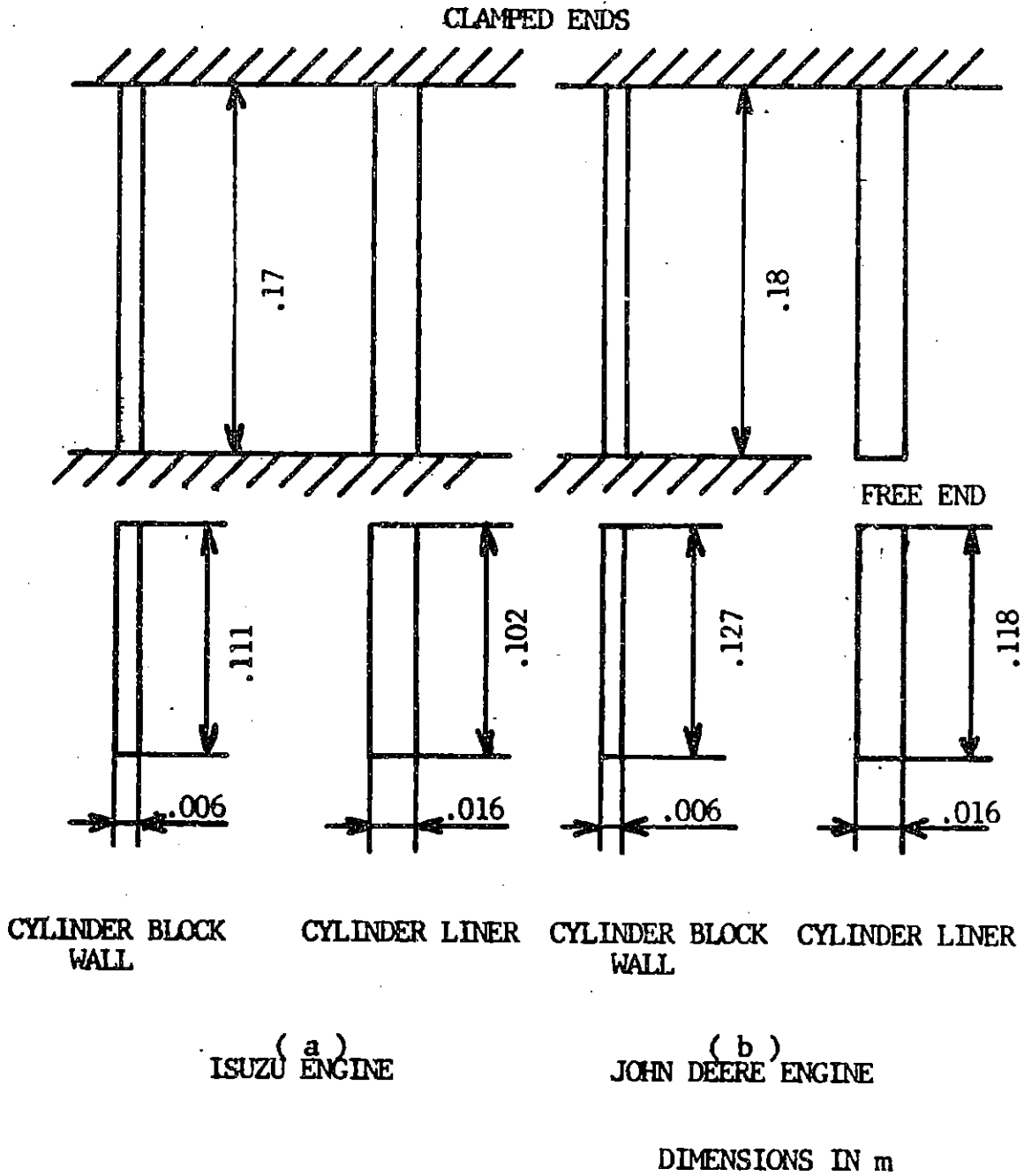JOHN DEERE ENGINE

DIMENSIONS IN m

FIGURE 5.2   :   DIMENSIONS AND BOUNDARY CONDITIONS
OF THE BEAM MODELS
FOR THE CYLINDER BLOCK

ENGINE	BEAM WHICH REPRESENTS	NATURAL FREQUENCIES (Hz)		
ISUZU C240	CYLINDER LINER		2900	7990
	CYLINDER BLOCK WALL	1090	3000	5880
JOHN DEERE 4219DF	CYLINDER LINER	410	2550	7130
	CYLINDER BLOCK WALL	970	2670	5250

TABLE 5.1 : NATURAL FREQUENCIES OF THE BEAM MODELS

REFERENCES

1. Mason, R. L., "Progress in the Reduction of Diesel Engine Noise," Sound and Vibration, Vol. 8, No. 2, February, 1974, pp 16-19.

2. Damkevala, R. J., Manning, J. E., and Lyon, R. H., "Noise Control Handbook for Diesel-Powered Vehicles," DOT-TSC-OST-74-5, April, 1975.

3. Gibbs, H. G., and Richards, T. H., "Stress, Vibration and Noise Analysis in Vehicles," Halsted Press, John Wiley & Sons, 1975.

4. Zimmermann, K. D., "Injection Noise and Its Relation to Fuel Pump and Engine Noise," SAE Paper 750802, (SP-397), 1975, pp 89-100.

5. Swanson, I.N., "Air Intake Silencing for Small Engines," SAE Paper 750751, 1975, 6 pp.

6. Monaghan, M. L. and McFadden, J. J., "A Light Duty Diesel for America?", SAE Paper 750330, 1975, 11 pp.

7. Anderson, D., and Baker, J., "Influences of Operating Cycle on Noise of Diesel Engines," SAE Paper 730241, 1973, 12 pp.

8. Russel, M. F., "Recent CAV Research into Noise, Emissions and Fuel Economy of Diesel Engines," SAE Paper 770257, 1977, 16 pp.

9. Bassoli, C., Cornetti, G.M. and Levizzari, G., "Combustion Noise and Ignition Delay in Diesel Engines," SAE Paper 770012, 1977, 10 pp.

10. Strahle, W. C., and Handley, J. C., "Stochastic Combustion and Diesel Engine Noise," SAE Paper 770408, 1977, 12 pp.

11. Taylor, C.F., "The Internal Combustion Engine in Theory and Practice", The MIT Press, 1968.

12. Bishop, G.R., and Leavitt, A. H., "Performance Simulation of a Diesel Piston and Ring System", SAE paper 750768, 1975, 12 pp.

13. Laws, A.M., Parker, D.A., and Turner, B., "Piston Movement in the Diesel Engine", CIMAC Congress, 1973, pp. 809-833.

14. Haddad, S.D., and Pullen, H.L., "Piston Slap as a Source of Noise and Vibration in Diesel Engines", Journal of Sound and Vibration, Vol. 34, No. 2, 1974, pp. 249-260.

REFERENCES (CONTINUED)

15. Haddad, S.D., Pullen, H.L., and Priede, T., "Relation Between Combustion and Mechanically Induced Noise in Automotive Diesel Engines", 15th FISITA Congress, Paris, paper A-2-4, 1974.

16. Haddad, S.D., "Liner Deformation Due to Piston Slap in Diesel Engines", I. Mech. E., 1975, pp. 1065-1071.

17. Haddad, S.D., and Fortescue, P.W., "Simulating Piston Slap by an Analogue Computer", Journal of Sound and Vibration, Vol. 52, No. 1, 1977, pp. 79-93.

18. Haddad, S.D., "Study of Diesel Engine Noise and Vibration Sources using Simulation Techniques", 16th FISITA Congress, Tokyo, 1976, pp. 3.31 - 3.39.

19. Ungar, E.E., and Ross, D., "Vibration and Noise due to Piston-slap in Reciprocating Machinery", Journal of Sound and Vibration, Vol. 2, No. 2, 1965, pp. 132-146.

20. Griffiths, W.J., and Skorecki, J., "Some Aspects of Vibration of a Single Cylinder Diesel Engine", Journal of Sound and Vibration, Vol. 1, No. 4, 1964, pp. 345-364.

21. Maples, V., "On the Frequency Content of the Surface Vibration of a Disel Engine", Journal of Sound and Vibration, Vol. 52, No. 3, 1977, pp. 365-386.

22. Skobtsov, E.A., Izotov, A.B. and Tuzov, L.V., "Methods of Reducing Vibration and Noise in Diesel Engines", National Lending Library for Science and Technology, 1966.

23. Rohrle, M.D., "Affecting Diesel Engine Noise by the Piston", SAE paper, 750799 (SP-397), 1975, pp. 51-67.

24. Usami, T., Wada, S., and Sonoda, S., "Piston Slap Noise of IDI Diesel Engine", SAE paper 750801, (SP-397), 1975, pp. 80-88.

25. DeJong, R.G., "Vibration Energy Transfer in a Diesel Engine", ScD. Thesis, MIT, Dept. of Mech. Eng., 1976.

26. Lyon, R.H., "Statistical Energy Analysis of Dynamical Systems", The MIT Press, 1975.

27. Laylor, N. and Petyt, M., "Modes of Engine Structure Vibration as a Source of Noise", SAE paper, 750833 (SP-397), 1975, pp. 120-133.

28. Beranek, L., "Noise and Vibration Control", McGraw-Hill Book Company, 1971.

29. Morse, P.M. and Ingard, K.U., "Theoretical Acoustics", McGraw-Hill Book Company, 1968.